UNIVERSITY OF TURKU

Transferability of process parameters and material feedstock between different metal additive manufacturing systems

Materials Engineering
Master's thesis

Author:
Niklas Lind

24.3.2025
Turku

Master's thesis

Subject: Materials Engineering
Author: Niklas Lind
Title: Transferability of process parameters and material feedstock between different metal additive manufacturing systems
Supervisors: Adjunct professor Heidi Piili, D.Sc. (Tech), Jukka Simola, M.Sc
Advisors: Hannu Heikkinen, M.Sc, prof. Antti Salminen, Emilia Palo, PhD
Number of pages: 88 pages
Date: 24.3.2025

Additive manufacturing is a relatively new manufacturing technology that is revolutionizing the way that parts for certain applications are manufactured. Additive manufacturing of metals solves many problems that traditional manufacturing methods have had by being able to build internal channels for example that would in other ways be impossible to produce.

The aim of this thesis is to research how well a metal powder designed to be used in a specific system performs in a system it was not designed to be used in. The aim is also to find out how well the process parameters from one system works in the other system and what changes need to be done to achieve the same results if any.

The study was conducted using three different materials, aluminium AlSi10Mg, stainless steel AISI 316L and cobalt chrome MP1. The materials were provided by Electro Optical Systems in addition to the other AlSi10Mg material used that was provided by SLM Solutions. The system that this study focused on was an SLM Solutions 280HL owned by the Turku University of Applied Sciences.

The tested parts of AlSi10Mg and MP1 were manufactured using the process parameters developed by SLM Solutions and the 316L samples were manufactured using the process parameters developed during this study based on the parameter tests conducted with the help of the material experts at EOS.

From the results it can be concluded that the transferring of the material feedstock was successful as the resulting part properties matched or even in some cases exceeded the properties that the results were compared.

Key words: Additive manufacturing, AlSi10Mg, 316L, MP1, PBF-LB/M, Laser-based powder bed fusion, Metal,

Acknowledgements

This thesis was carried out at Electro Optical Systems Finland Oy from May of 2024 to March of 2025. I want to thank my supervisor Jukka Simola for the invaluable support during the thesis process. I also want to thank Hannu Heikkinen, Eero Virtanen, Antti Seppälä and Juha Ottelin, for the support and help with every possible question that I have had trouble with. Huge thanks also to the operators Aki and Kauko who helped me with the logistics and post processing steps as well as to all the amazing people in the laboratory that assisted me.

I also want to thank my supervisor from the University of Turku, Heidi Piili for all the assistance and feedback to make this thesis possible. Huge thanks to my advisors Antti Salminen and Emilia Palo from the University of Turku. Thank you also belongs to Pekka Törnqvist from the Turku University of Applied Sciences who taught me the know-how on their systems.

Last but not least I want to thank Inka and my family for the love and support during the process. Thanks to my friends for supporting me and helping take my mind off of things when I have needed it the most. Special thank you belongs to my emotional support dog Cava who has always brightened my day.

Table of contents

Nomenclature

Abbreviation	**Explanation**
AlSi10Mg	Aluminium alloy
AM	Additive manufacturing
PBF-EB/M	Powder bed fusion of metal with an electron beam
HBR	Brinell hardness
HV10	Vickers hardness, 10 kg paino
IN718	Nickel based alloy
LOF	Lack of fusion
MP1	Cobalt chrome alloy
PBF-LB/M	Powder bed fusion of metal with a laser beam
AISI 316L	Stainless steel grade

Symbol	**Explanation**
d_h	Hatch distance (mm)
HI	Volumetric heat input (J/mm^3)
P	Laser power (W)
Ra	Arithmetical mean height of a profile (mm)
Sa	Arithmetical mean height of a surface (mm)
t	Layer thickness (mm)
v	Laser beam scanning speed (mm/s)

1 Introduction

1.1 Research problem

Additive manufacturing is a fast-growing technology field that offers possibilities that are impossible on more conventional manufacturing methods. Additive manufacturing is especially useful in cases where complex designs are used where traditional manufacturing methods would be extremely hard to implement. (Bassoli et al., 2021) Even though the field of AM is growing at a huge speed, there are some challenges that are yet to be resolved.

The materials used in additive manufacturing can in some cases be developed with specific machines in mind. This causes lack of knowledge on how well the material performs in a system that it was not designed to be used in. The same problem occurs with the process parameters as the differences in the materials or the systems themselves can be minimal, the effect on the processability of the materials are not known and can thus cause major differences in the performance (Cortis et al., 2023). Part properties are not directly derived from the alloy composition in AM, but are inherently linked to the parametrization of the build process and other physical properties of the powder, making the optimization of the parameters for a specific system and powder combination important.

1.2 Objective of the thesis and research questions

The objective of this thesis is to study how well the materials made by a company for specific systems work when used in a system made by third party company when compared to the performance of their own materials. Objective is also to have a comparison between the two systems discussed in this thesis from the perspective of an operator.

Motivation for this thesis comes from the lack of knowledge of how well a material performs in a third-party system if it has been developed for systems of one company. This would provide knowledge for material manufacturers about the performance and if the materials could be used in different systems. This also enables customers who use several systems to have the confidence to run multiple brands of AM systems with the same powders, thus reducing the complexity of warehousing separate materials for different systems.

Focus on this thesis is on the bulk material of the parts (infill), i.e. the amount of porosity that the built parts have. The focus is on the infill because it is a

Research questions on this thesis are:

- How well can material feedstock be used in different systems.
- What changes in the infill parameters need to be done to get good results.
- What it takes to create a new process for a system
- What are the key differences between systems and their operation

1.3 Scope and structure of the thesis

This thesis consists of a literature part and an experimental part. The literature part gives a base of knowledge about the general field of AM and in-depth knowledge about the specific subject of this thesis.

The experimental part focuses on three materials. Aluminium alloy AlSi10Mg, Cobalt-Chrome alloy MP1 (comparable to CoCr28Mo6) and Stainless-Steel alloy 316L. Aluminium is made on the system B using powder from two different manufacturers, whereas stainless steel and cobalt-chrome is made using only one powder. The results of the parts are compared to reference results of parts made on system A that the powders are developed to be used on.

2 Processability of materials in PBF-LB/M

PBF-LB/M (powder bed fusion of metal with a laser beam) introduces possibilities in manufacturing complex parts that have not been possible with traditional manufacturing methods. The leading industries implementing additive manufacturing in their processes are automotive, aerospace, medical and dental industries, while oil and gas, electronics, construction and railway industries are raising their interests. (Vafadar et al., 2021) To fit the needs of each interested industry, multiple materials have been developed to fit the needs from the industrial side of mechanical and corrosion resistance properties for example.

2.1 Aluminium

High strength aluminium alloys are used in AM for their excellent strength to weight ratios as well as being inexpensive compared to some other alternatives (Aboulkhair et al., 2019). Aluminium alloys are also widely used in AM because of the high production rates of the processes for Aluminium. There are however drawbacks in the high production rate processes because of defects in the final products, although this has improved in the last years because of big investments in from especially the aerospace industry (Altıparmak et al., 2021). Now it is possible to produce near full relative density parts when the processing conditions are optimised (Kotadia et al., 2021). Other advantage in additively manufacturing aluminium alloys are the improvements to the microstructure compared to the cast aluminium alloys. Cast alloys require chemical additives to reach certain level of microstructure, but in AM, the high cooling rates improve the microstructure without having to alter the chemistry of the alloy (Aboulkhair et al., 2019).

Advantage in the use of Al-Si-Mg alloys is the improved corrosion resistance compared to the cast material counterparts (Michi et al., 2022). AlSi10Mg is widely used because of its excellent properties compared to the weight of the material. Using additively manufactured AlSi10Mg follows a similar path as other early adopted additive manufacturing materials, being originally an established casting alloy. (Electro Optical Systems GmbH, 2024a)

2.2 Stainless steel

In additive manufacturing, one of the most used stainless steel materials is 316L. It is a high performance austenitic stainless steel that has excellent properties to be used for example in the

automotive industry. 316L is also widely used in the chemical industry where corrosion resistance in high temperatures is needed. (D'Andrea, 2023; Electro Optical Systems GmbH, 2024d)

316L has remarkable corrosion resistance and the welding capabilities are excellent. Additively manufactured 316L consists of a network of 3-dimensional cells, borders of which are enriched in Cr, Ni, Mo, Si and Mn. The borders are also depleted in Fe. It can be observed that these borders are highly resistant to corrosion (Revilla et al., 2020). Stainless steel has a habit of producing residual stresses during the additive manufacturing process that can cause cracks into the microstructure. These residual stresses and cracks can however be minimised by optimizing the process parameters. (Wu et al., 2014)

2.3 Cobalt chrome

Cobalt chrome alloys are widely used in the medical industry because of the characteristics of the material needed in the medical field. These characteristics are biocompatibility to chemical compositions in the human body and high corrosion resistance inside the environment of the body (Mordas et al., 2020).

The key advantage of additively manufacturing cobalt chrome compared to conventional cast parts is the improvement in mechanical properties. Largest contributor to the enhanced mechanical properties is the significantly smaller grain size of additively manufactured material (Hong & Yeoh, 2020).

MP1 is Cobalt chrome material for additive manufacturing. MP1 is used because of the excellent corrosion resistance and great mechanical properties that are present even in elevated temperatures. MP1 is also nickel free, which makes it ideal for applications in the medical industry. (Electro Optical Systems GmbH, 2024b)

3 Existing studies on system comparison

Powder manufacturers that also produce additive manufacturing systems usually develop the materials using only their own systems. This causes there to be lack of studies on how well the powders developed by using a specific system behave when used in a system of a different manufacturer. Multiple research papers have however been made where different machines are compared against each other.

Medrano et al. studied the tensile test results of AlSi7Mg parts manufactured using EOS M290 and SLM 280HL. AlSi7Mg (F357) is similar to the AlSi10Mg powder used in this thesis, with the main difference being the smaller fraction of silicon in AlSi7Mg. The study used AlSi7Mg from different suppliers in the machines. F357 from IMR metal technologies was used in the SLM 280HL and F357 from Valimet used in the M290. The study also experimented with different heat treatment methods and treatment times. The study also has density measurements, microstructure characterization and hardness measurements done on the parts. Conclusions from this study were that the machine differences do not affect the produced parts significantly, and any small differences are erased with the heat treating. Another conclusion was that the aging temperature has more effect on the parts than aging time. (Medrano et al., 2023)

Obeidi et al. compares porosities and mechanical performance of 316L in different AM systems. The systems used in this study were Aconity MINI, Phenix 3D Systems ProX 200, EOS M280 and Concept laser M1 Cusing. All of these systems were using the same powder manufactured by Carpenter Additive, to rule out the error caused by the variance between materials. In all cases 30 µm and 60 µm layer thicknesses were tested. The densities of the parts were tested using the Archimedean method. Densities of the parts were measured to be highest in the parts made with the EOS M280 and Aconity MINI systems. Densities of parts made with the Concept Laser system were generally the lowest, but this was thought to be because of nitrogen was used as the shielding gas instead of argon as with the other systems. With additively manufactured stainless steel, it is studied that the porosity is higher when more nitrogen is present in the shielding gas (Yang et al., 2021). Best tensile test results were achieved with the EOS M290, followed by the systems of Aconity, Phenix 3D systems and lastly Concept Laser. The results in parts manufactured with a layer thickness of 30 µm were relatively close to each other but in the 60 µm parts, the difference in results was more significant, depending on the parameter values used. In the worst case the difference of tensile strengths was around 700 MPa on the M280 to around 200 MPa on the parts made with Concept Laser machine.

During the analysis of the pores in the manufactured parts, it was noticed that the parts produced with the EOS M280 showed a fully solid grain structure, with pores only noticeable on the grain boundaries, whereas the parts manufactured with the other systems, porosity was noticed throughout the cross-sectional area. It is also said in the study that because the process is a thermal process, the mechanical properties are affected by the heating and cooling rates of the material. These rates are affected by the volume of the build chamber and temperature of the build platform, but also by the circulation of the shielding gas. (Ahmed Obeidi et al., 2021)

Uriati (2022) and Nicoletto (2022) have studied the differences of additively manufactured Inconel 718 with different PBF-LB/M systems (Uriati & Nicoletto, 2022). The used systems in the study were SLM 280HL, EOS M290 and Renishaw AM250. They found out that the fatigue strength of the test parts had large differences depending on the build orientation of the parts, highlighting the importance of optimizing the process conditions for the whole production process. The largest differences in the fatigue strength on the same orientation was found to be 260 MPa compared to 450 MPa (Uriati & Nicoletto, 2022).

Moshiri et.al. have conducted a benchmarking study on different laser powder bed fusion machines. The study was done by having five state-of-the-art machines being run by their respective manufacturers and two state of the art machines run by the end users. One of the machines operated by the end user was significantly older than the rest of the machines and this older one was identified to be the EOS M270. All the machines were used to build the same part geometries that were then tested for their properties. It was observed that the newer machines were not able to outperform the older M270, emphasizing that experience and expertise are important factors in the final results. It also highlights that the trend of newer systems is to focus on the ability to build even larger parts with faster systems, with the main contributor to the build speed being the addition of multiple lasers working together. The results between the machines were more or less the same throughout the experiment with a few outliers for example in the surface roughness of the parts. (Moshiri et al., 2019)

4 Process parameters and part properties affecting transferability

In order for the transferability of the materials to be successful, the system that the material was transferred to has to be able to reproduce the key properties of the material on a similar level that the system the material was developed for is capable of. The material properties that are characterized are: tensile properties, hardness, porosity, corrosion resistance, surface roughness etc. Some of the properties can be altered by changing the manufacturing or post-processing steps to meet the requirements of some specific application.

Transferability of material feedstock is dependent on the parameters and the whole setup that the material is transferred to. In this chapter it is defined what are the key functions and parameters that need to be optimised in the process and in the final products so that it can be said that the transfer is possible.

4.1 Process parameters

4.1.1 Laser power

With suboptimal laser power, multiple problems could occur. In the process, Lack-of-Fusion in the process could occur, which means that the laser power is not high enough to melt all the powder, which leads to unmelted particles in the bulk material. This causes in turn defects in the material as the particles have not fused together. Gas pores could occur when the laser power is too high, causing the low melting phases to vaporize. The gases can get trapped into the otherwise melted material and leave characteristic spherical shaped gas pores to the bulk material (Muñoz, 2017). Laser power in companion with the hatch distance are the two parameters that have the most impact on the final quality of the product. Laser power being the most important, as the laser is not able to melt the powder even if the hatch distance is low if the laser power is not high enough (Choudhury et al., 2023).

4.1.2 Hatch distance

Hatch distance is the parameter describing the distance between individual laser vectors in PBF-LB/M process. Hatch distance greatly affects the final quality of the part and also the time it takes for the process to finish. The hatch distance needs to be small enough that the tracks melted and solidified by the laser vectors overlap enough for the resulting part to be solid without defects, but it need to be big enough so that the process is not unnecessarily slow. If the hatch distance is too big, the melt pools will leave gaps between them, resulting in porous

material or unmelted particles within the final product, compromising the mechanical properties of the product. When the hatch distance has only a small deviation from the optimal distance, it has very little effect on the build quality of the parts, the larger effect is on the processing time. (Muñoz, 2017)

Figure 1 shows the hatch distance between adjacent laser vectors.

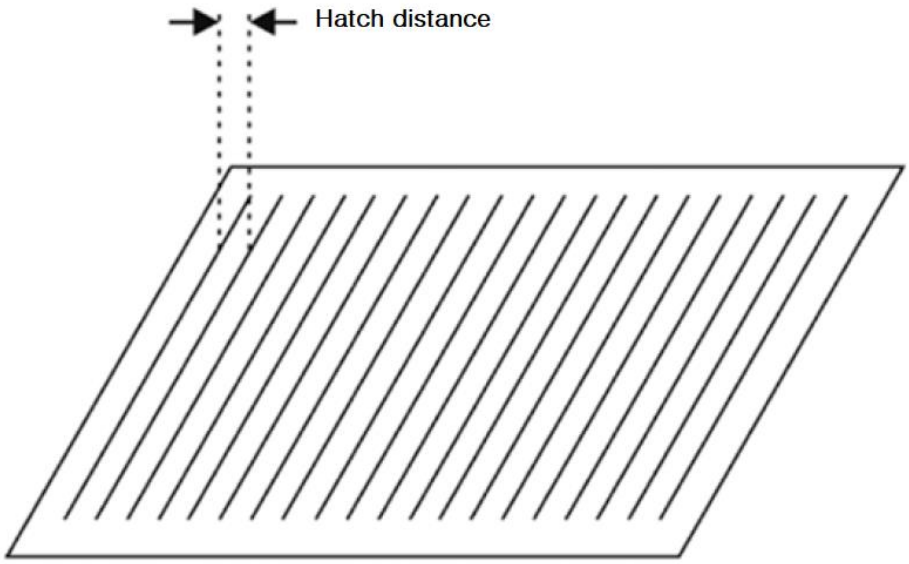

Figure 1. Hatch distance between adjacent laser vectors. Reproduced from (Volpato et al., 2022) which is under an open access Creative Common CC BY license.

Figure 1 (Volpato et al., 2022) illustrates the hatch distance, showing that it means the distance between two adjacent laser beam movement vectors.

Hatch distance is a key contributor to the mechanical properties of the part. Especially tensile strength and elongation of the material are affected by the changes in the hatch distance because of the defects that can be formed in the structure of the part (Zhang et al., 2023).

4.1.3 Heat input

Heat input is the amount of energy brought to the powder from the laser. It is calculated by using the laser power, hatch distance, laser scanning speed and the layer thickness. The equation for calculating the heat input (*HI)* is shown in Equation 1.

$$HI = \frac{P}{v \times dh \times t} \quad (1)$$

Where P is the laser power, v is the scanning speed of the laser, d_h is the hatch distance and t is the layer thickness. The unit of volumetric heat input (HI) is J/mm^3. (Yonehara et al., 2020)

The heat input needed is depended on not just the chemical composition of the material, but also the particle size distribution of the powder. The larger particle sizes the powder has; the more energy is needed to melt the powder.

Heat input also plays a role in the amount of defects, because the scanning speed of the laser beam in this thesis is dependent on the heat input, because in this thesis the heat input was varied with the power and hatch distance resulting in different scanning speeds, whereas in some cases the scanning speed might be decided resulting in different heat inputs. If the laser power and hatch distance are optimized, but the heat input is low, causing the scanning speed to be high, the laser beam does not bring enough energy to the powder for it to melt properly.

Heat input as well as the other parameters are usually chosen in a way that the actual quality of the parts is good enough, but also in a way that the process does not take too long to complete. (Hitzler et al., 2017)

4.1.4 Shielding gas

Shielding gas plays a crucial role in the additive manufacturing process to keep oxygen away from the process, and to also carry the spatter away from the powder bed. The type of shielding gas varies, and the choice of shielding gas is important to consider. For example with stainless steel such as 316L, argon gas (Ar) is the preferred shield gas to use as the use of nitrogen as the shielding gas can result to porosity caused by the nitrogen getting trapped to the bulk material (Yang et al., 2021). However the inert shield gas has little to no effect on some materials such as aluminium alloys but while using shielding gas such as CO_2 that is not inert, defects cannot be ruled out (Kleemeyer, n.d.).

The shielding gas flow rate however affects the final products drastically. If the flow rate of the gas is too low, the flow does not carry the spatters from the process causing the laser beam to hit the fumes and oversized particles from the process. This results in lack of fusion porosity due to the lost laser beam energy caused by the process fumes, and the oversized particles that do not melt properly. (Reijonen et al., 2020)

4.2 Part properties

4.2.1 Scrap rate

Scrap rate in additive manufacturing is the volume of powder that goes to waste in the building process. The scrap rate is calculated using the Equation 2.

$$1 - \frac{\Delta Bp}{\Delta P} * 100\% = scrap\ rate \quad (2)$$

Where ΔBp is the difference in the weight of building platform before and after the building process and ΔP is the difference in the weight of the powder before the process and after the process and sieving. Scrap rate is usually mentioned as percentage of the starting weight of the powder.

Scrap rate is important in the build process as it directly contributes to the cost of the operation of the system. The more powder goes to waste, the more the user needs to purchase the powder for the same number of parts. Scrap rate is also important from the environmental aspect as the more times the powder can be reused, the less there is need to produce and buy more powder. Nowadays, when the sustainability of products is brought up more and more, scrap rate becomes even more relevant as companies aim for sustainability and cost savings (Hegab et al., 2023; Peng et al., 2018).

4.2.2 Porosity

There are three main types of microstructural porosity that exist in AM parts: lack of fusion (LOF) porosity, gas porosity and high-energy porosity. (Vastola et al., 2018)

Lack-of-fusion porosity occurs when the energy supplied by the laser beam is not enough to melt all the metal powder, which leads to unmelted particles among the otherwise uniform solid material and layers that are not fused together. Lack-of-fusion pores can be identified by their elongated shape that is oriented horizontally along layer boundaries. Lack-of-fusion defects have the most effect on the mechanical properties of the component. (Sola & Nouri, 2019)

Gas porosity occurs when the gas trapped in the powder feedstock is encapsulated in the final solid form of the part. This usually happens with powders that are gas-atomized but not in powders that are for example plasma-atomized. Thes pores are also called spherical pores, because they are usually completely round. (Sola & Nouri, 2019)

The final type of porosity, high-energy porosity happens when the energy provided by the laser is too high and the particles end up vaporizing and leaving behind keyhole porosity (Sola & Nouri, 2019). Porosity affects the mechanical behaviour of the final products. Especially fatigue life of a product is greatly affected (Sola & Nouri, 2019). There can be multiple types of porosities in a single sample, for example lack of fusion porosities and gas porosities can exist in the same object (Kim et al., 2017).

One contributor to the amount of porosity in the finalised product is the flow speed of shielding gas during the process. When the flow speed is too low, the vapours from the process drastically decreases the effective laser energy that reaches the powder bed and causes lack of fusion porosities (Reijonen et al., 2020).

4.2.3 Density

Density of additively manufactured material is always compared to the theoretical density of the material, that is calculated from the chemistry of the material. The density of the product is comparable to the number of defects that it has as the higher porosity of the solid is, the less dense it is. Density is related to discontinuities in the microstructure, such as porosity and other defects, and is therefore in direct relation to the mechanical properties of the part. In recent years, machine learning has been utilised to further improve the density of parts by optimizing the process parameters through analysing earlier results. (Gor et al., 2022)

4.2.4 Surface roughness

Surface roughness means the multitude and size of the deviations from the mean level of a surface. In AM the surface roughness of a part has always been an issue because of the irregularities in the melt pool during the production of the parts.

Surface roughness can be indicated in many ways, but the best overviews of the actual roughness are shown with Ra (Roughness average) and Sa (Arithmetical mean height) values. Ra value is determined by a single profile from the surface, where the measuring device determines the mean of the profile and calculates the average deviation from the mean on that profile. Sa on the other hand is determined from the whole studied surface by determining the mean and the deviations on every point of the surface. Because of these analysis types, the Ra value can deviate a lot depending on the exact location from where the profile is located. Sa analysis does not have the same problem because it considers the whole surface of the part.

One of the most significant influences on the surface roughness of a part comes from the layer thickness of the process. This is because when the layers are thicker, the melt pool during the process is more inconsistent resulting in a rougher surface than on a lower layer thickness (Cao et al., 2021). Surface roughness also changes according to the laser power being used, as well as the speed of the laser beam being moved. When these parameters are changed, resulting in an optimal heat input, the surface roughness lowers (Whip et al., 2019).

Surface roughness of a part can be improved by remelting the surface of the part after the initial exposure. This has drastic changes on the Ra values measured from the surfaces. In the remelting, high heat inputs are to be avoided so that the formation of gas defects can be avoided. (Boschetto et al., 2021)

5 Aim and purpose of experimental part

Aim of the experimental part is to achieve a comprehensive view on how well selected materials and parameters work when transferred from one machine to another. In this case the aim is to achieve this view in bringing EOS powder and parameters to an SLM machine, not the other way around although this would be a subject worth studying in itself.

Purpose of the experimental part is also to figure out how to create a new process to a system. The purpose is to study what need to be done in order to create a new process for a material and experiment if the process developed is successful. Also, in the case of 316L, the purpose is to create a new process for this material because there was no active license for the parameters to be used in the study.

6 Experimental set up

6.1 Hardware

6.1.1 EOS M290

EOS M290 is a well-established mid-to-small format machine in the current system landscape of PBF/LB-M, where build envelopes range from Ø 100 x 95 mm (EOS M100) to 800 x 800 x 1200 mm (AMCM M 8K) (Inovar Communications Ltd, 2023).

The building chamber of the M290 250 x 250 x 345 mm. The M290 has one 400W laser. (Electro Optical Systems GmbH, 2024c) The M290 has three compartments in the build chamber. Right-most is a dispensing unit, middle one is the build envelope and the one on the left is for the excess powder that the recoater has taken from the dispenser and cannot fit on the building platform.

The EOS M290 offers the widest range of validated materials on the market, to fulfil a wide range of customer needs. (Electro Optical Systems GmbH, 2024c)

Figure 2 shows the EOS M290 PBF-LB/M device used in this thesis.

Figure 2. PBF-LB/M device EOS M290 used in this thesis

EOS M290 is shown in Figure 2. In the figure, the main part of the system is in the middle, the controlling panel is on the right and the filtering unit of the circulating atmosphere is on the left.

6.1.2 SLM 280HL

The 280HL is the mid-size machine of SLM Solutions. It is machine in the catalogue of SLM that is directly comparable to the EOS M290 because of the similarity in the technology and the size of the build envelope

The build envelope in this machine is 280 x 280 x 365 mm so it is 30 mm per side bigger and 20 mm higher than the build envelope on the EOS M290.(Electro Optical Systems GmbH, 2024c; SLM Solutions, 2024) Laser options for the 280HL are one or two 400W lasers, one or

two 700W lasers, or a combination of one 700W laser and a 1000W laser.(SLM Solutions, 2024) Both 280HL systems used in this thesis had two 400W lasers.

One of the selling points in the SLM 280HL is the possibility to handle the powder in oxygen free atmosphere. The 280HL also offers the possibility to remove the overflow of powder from the machine, sieve the powder and bring it back to the machine while the process is still ongoing. (SLM Solutions, 2024)

Figure 3 shows one of the two SLM 280HL systems used in this thesis.

Figure 3. SLM 280HL system used in this thesis

From Figure 3 it can be seen that the composition of the system is similar to the EOS M290. The main compartment is on the middle, the control panel on the right and the filtering system on the left.

6.1.3 Analysis of systems

One of the main differences of the systems is the bi-directional recoating in SLM 280HL. In M290, the recoating happens always from the right to left whereas in the 280HL, the recoater

moves from back to the front direction in relation to the build chamber. Flow direction is also different in the systems. In the M290 the gas flow is from the back of the chamber to the front towards the detachable extraction nozzle at the chamber door. On the 280HL the flow direction is from right to left.

Operation on the systems is also quite different. The design of the M290 is more open than the 280HL as the powder is in open chambers on the same level as the build platform. Because of the more open design, meaning the access to the powder reservoir is easier in the machine. On the 280HL it was noticeable how challenging the powder handling sometimes was when the powder had to be lifted on top of the machine and turned upside down while fastening the container to a pipe that leads the powder to the dispensing system. whereas on the M290 the powder is poured directly through the opening of the build chamber.

Figure 4 shows the side-by-side pictures of the M290 and 280HL building chambers.

Figure 4 Side-by-side pictures of M290 building chamber on the left and 280HL on the right

As it can be seen from Figure 4, the orientation of the recoaters are different and the gas flow on the M290 is from the back to the front whereas on the 280HL, the gas flows from the right to the left.

The emptying and clean-up of the machine in the exact configuration used in this thesis was more difficult on the 280HL because the powder had to be brushed off the building platform into the collector chambers. The powder can be brushed from the build envelope using the glove

box incorporated on the build chambers door, but the holes to the gloves are relatively small so in my own experience it is easier to just do it with the door open. This however makes the handling of the powder in oxygen free environment impossible and requires the user to wear protective equipment for this task. Taking the powder from the collector chambers was not easy either as the operators must be on their knees while inserting the container below the collecting chamber and hitting the chamber with a plastic hammer to get the powder flowing out of the chamber. There is also no fool-proof way of knowing if all the powder has come out of the chamber as there are no sensors in the chamber and visual inspection of the collecting chamber is not possible without any additional equipment. This causes there to sometimes be powder left over in the chamber even though the operator thinks that process has been done thoroughly.

6.2 Software

Pre-processing of CAD data includes using a slicer software to give layer by layer information on the area to be exposed by laser at each layer. On EOS machines, EOSPRINT is used, which is a software developed by EOS. On the SLM machines, in this case, Siemens NX is used with a Materialise Magics add-on. Both software can be used to position the parts on to the building platform and to set the parameters and building order for each part.

6.2.1 Comparison of the slicing software

Both slicing software have similar workflows. First a correct type of build envelope is opened, after which the parts are added onto the platform area. EOSPRINT differs from NX slightly by giving option to choose the material straight from the main window of the software whereas in NX material is chosen from the same pop-up window where you choose the building strategies from. Choosing the building strategy is done similarly in both software and different strategy can be chosen for each individual part or just as easily use the same strategy for every part.

Using the software, some problems came up when trying to upload some parts into NX. The software was precise about the models not having any errors in the surfaces, because then it will not recognise them as a bulk body of material, but only as a surface, which cannot be uploaded to the build file. When uploading the same file to EOSPRINT, there were no issues. With NX, another problem was noticed when attempting to upload the job into NX as individual

parts. The software did not recognize the placement of the parts that were predefined in Materialise Magics and just placed all the parts to the middle of the platform. This same problem did not come up when tested on EOSPRINT. The problem was overcome by simply merging all the parts as one STL file and then uploading it into NX but after the parts are merged, it blocks the moving and modifying of individual parts in Magics. Giving separate sections of merged parts individual exposure parameters was still possible when the STL file was uploaded to NX.

6.3 Materials

6.3.1 AlSi10Mg

Two different AlSi10Mg aluminium powders were used in this thesis. One was supplied by EOS and the other by SLM. The two powders are almost identical comparing their chemical composition shown in Table 1 and Table 2. The main difference of the powders comes from their particle size distribution. The general particle size distribution on the EOS powders is 25-70 µm and on the SLM powder the general particle size distribution is 20-63 µm. However, the EOS powder has a larger proportion of fine particles compared to SLM powder which influences the powder behaviour inside the machine during the process.

Table 1 EOS AlSi10Mg chemical composition from the MDS (wt.-%)

Element	Min.	Max.
Al	Balance	
Si	9.00	11.00
Fe	-	0.55
Cu	-	0.05
Mn	-	0.45
Mg	0.25	0.45
Ni	-	0.05
Zn	-	0.10
Pb	-	0.05
Sn	-	0.05
Ti	-	0.15

Table 2 SLM AlSi10Mg chemical composition from the MDS (wt.-%)

Element	Min.	Max
Al	Balance	
Si	9.00	11.00
Mg	0.20	0.45
Fe	-	0.55
Mn	-	0.45
Ti	-	0.15
Zn	-	0.10
Cu	-	0.05
Ni	-	0.05
Pb	-	0.05
Sn	-	0.05
Others	-	0.15

As the powders are quite similar in the ways presented in Table 1 and Table 2, the hypothesis is that the EOS powder will work without any bigger problems in the SLM 280HL. Some optimizations of the parameter values would most likely be in order but the standard process of SLM should work just fine.

6.3.2 Cobalt-Chrome

The experiments on Cobalt-Chrome were done using only the Cobalt-Chrome (MP1) from EOS. SLM does not have a product called MP1, but their CoCr28Mo6 product follows the same standards and is thus comparable to EOS MP1. The chemical composition of EOS MP1 can be seen from Table 3. The general particle size distribution of MP1 is 15 – 45 µm. General particle size distribution for the SLM's Cobalt material is 10 – 45 µm, so the difference between the powders is small.

Table 3 EOS MP1 chemical composition from the MDS (wt.-%)

Element	Min.	Max.
Co	60.00	65.00
Cr	27.00	30.00
Mo	5.00	7.00
W	-	0.20
Ni	-	0.10
Fe	-	0.75

Mn	-	1.00
Si	-	1.00
C	-	0.14

Table 4 SLM CoCr28Mo6 chemical composition from the MDS (wt.-%)

Element	Min.	Max
Co	Balance	
Cr	27.00	30.00
Mo	5.00	7.00
Mn	-	1.00
Si	-	1.00
Fe	-	0.75
Ni	-	0.50
C	-	0.35
Al	-	0.10
B	-	0.01
Ni	-	0.25
P	-	0.02
Si	-	0.01
W	-	0.20
Ti	-	0.10

Table 3 and Table 4 show that that the chemical composition of the powders are really close to each other, small difference being in the marginal materials that might be present in the SLM powder. Because the differences between the powders themselves are small, the expected outcome is that the EOS MP1 will work well in the SLM 280HL.

6.3.3 Stainless Steel

The experiments on Stainless steel were also done by only using material from EOS (316L). The chemical composition of 316L can be seen from Table 5. The general particle size distribution of EOS 316L is 20 – 65 μm.

Table 5 EOS 316L chemical composition from the MDS (wt.-%)

Element	Min.	Max.
Fe	Balance	
Cr	17.00	19.00

Ni	13.00	15.00
Mo	2.25	3.00
Cr	-	0.03
Ni	-	0.10

6.4 Test geometries

The geometries shown in Figure 5 and Figure 6 were built in the layouts to get the best possible view on the performance of the powder and parameters.

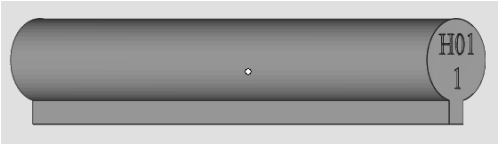

Figure 5. Horizontally built tensile test part (A)

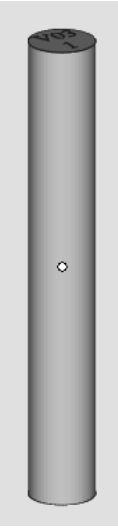

Figure 6. Vertically built tensile test part (B)

As it can be seen from Figure 5 and Figure 6, the geometries are identical apart from the support structure below the horizontal part in Figure 5.

Some of the tensile test parts were built horizontally and some were built vertically. This is done such that the effect of differently oriented layers in the finished part can be studied and

taken into account when manufacturing parts at the user's end. Tensile test parts are built as this kind of geometry in order to have the ability to machine the part to a certain geometry to correspond the geometry set in a specific material standard that the result is compared to.

Figure 7 the geometry used in density testing of the materials

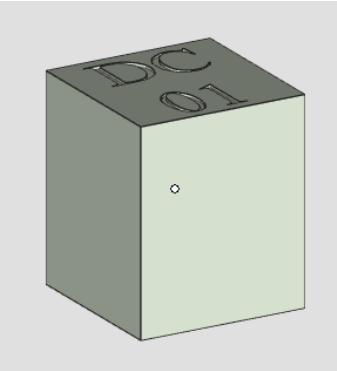

Figure 7. Density cube (C)

Density cubes were built to find out the density of the finished material using the Archimedean method. A simple cube was chosen for this so that the test would be easy to go through because in a more complex geometry, air bubbles could get stuck and thus affect the result of the Archimedean experiment.

Figure 8 shows the geometry used to test the hardness of each material.

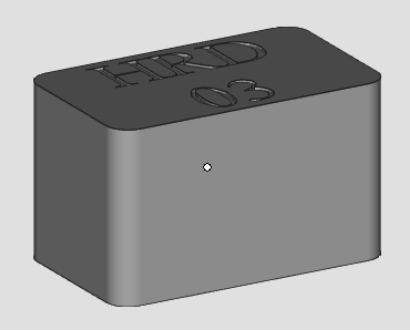

Figure 8. Hardness test part (D)

A simple design was chosen for the hardness test parts. The test does not require a complex geometry so a part that has simple straight sides was chosen. This part is ideal for hardness testing, because of the long sides that can be grinded smooth for the hardness testing to be conducted.

Figure 9 shows the geometry chosen to be used in the porosity testing.

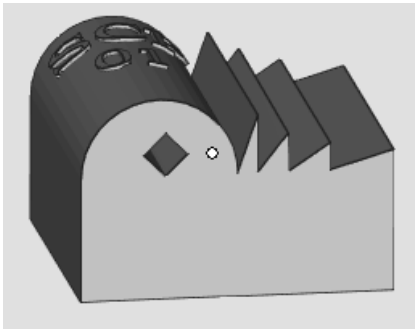

Figure 9. Porosity test part (E)

The part in Figure 9 is cut in half through the middle in order to study the internal defects in the bulk material. The part can also be modified to make the base higher or lower depending on how large of an area is desired to be observed.

Figure 10 shows the geometry used in the internal structures analysis and optical microscopy.

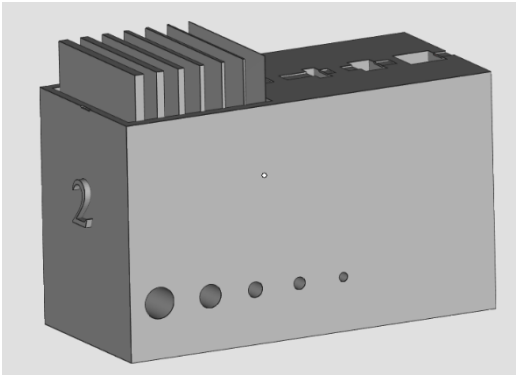

Figure 10. Thinwall and internal structures part (F)

The part in Figure 10 was chosen to see how well the system and material combination is able to build thin walls and internal channels. The part, when cut in half can be used to observe how consistent and thin the thinwalls in the structure are, as well as how well the ceilings of the internal channels at different angles have been built.

Figure 11 shows the part assembly used to measure the surface roughness of the parts.

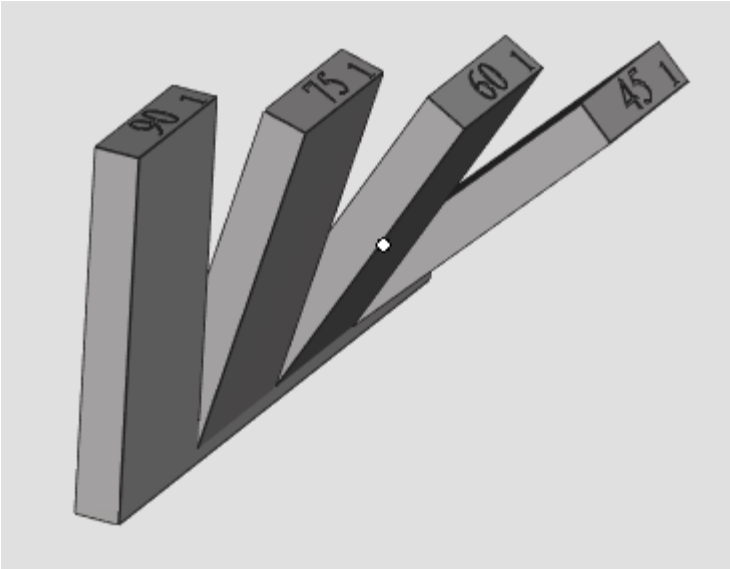

Figure 11. Surface roughness test part (G)

The part on Figure 11 is used to analyse the surface roughness of the parts in different building angles. This particular part has four different angles that are built, vertical, or 90-degrees, 75-degrees, 60-degrees and 45-degrees, in relation to the building platform. This geometry of the part allows the roughness to be analysed from both the upper and lower sides of the part to get the result from both upskin and downskin of the part. Upskin meaning the upper side of the part and downskin the down facing side o the part that is partly built on just the powder bed due to the orientation.

Figure 12 show the geometry used in the optical microscopy and etching tests of aluminium samples.

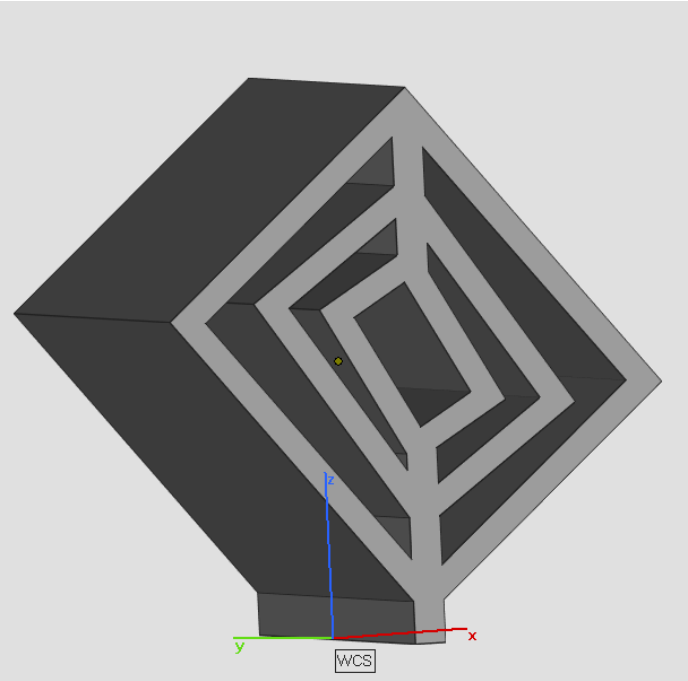

Figure 12. Downskin test part (H)

The geometry that is shown in Figure 12 is used to study the downskin of the part with the use of the different angles in the sides of the part. The part is cut in half in order to give a chance to observe surface roughness from the middle, where for example the contours from the sides of the part have no effect on the results.

6.5 Sample analysis tools

6.5.1 Porosity analysis

The porosity analysis parts were cut in half with an abrasive disc cutter. The samples were polished using the Struers Tegramin-30 sample polishing device shown in Figure 13. The actual analysis was done by using an Olympus GX51 optical microscope and an analysis software.

Figure 13. Struers Tegramin-30 sample polishing device

The Struers Tegramin-30 sample polishing device (Figure 13) is operated by the integrated controlling software in the machine. There are controlled recipes for each material that have been optimized in the laboratory to get the optimal polished surface with as few steps as possible. The polishing device is used by inserting a polishing disc or a grinding paper on the large spinning platform in the machine and putting the samples on the sample holder above the platform. Then the controlled recipe is started, and both the platform and the sample holder start spinning and the system drops either water or different diamond suspension liquids on the platform to help with the polishing.

Figure 14. Olympus GX51 optical microscope

After the samples are polished, the Olympus GX51 optical microscope shown in Figure 14 is used to produce the photos of the sample surface for the analysis. The sample is lowered to the top of the microscope and first a overall view of the sample area is taken with lower magnification lens, in order to get the right points of the samples to set the correct focus to the surface. Then with the higher magnification lens is used to take the images from the sample surface that are stitched together to achieve a high-resolution image of the whole surface, that can be analysed for the defects by calculating the area occupied by defects from the observed area of the sample.

6.5.2 Surface roughness analysis

The surface roughness analysis was done by using Alicona InfiniteFocus G5 shown in Figure 15.

Figure 15. Alicona InfiniteFocus G5

The equipment used in the surface roughness analysis is shown in Figure 15. The base of the machine is moveable from side-to-side, which gives the ability to image larger areas of a sample. The lenses on the system move up and down to focus the image on the correct height

6.5.3 Hardness analysis

Hardness analysis was conducted using the EMCO-Test DuraVision system, shown in Figure 16.

Figure 16. EMCO-Test DuraVision used in the hardness analysis

The system has a stand for the sample that move up and down. On top of the stand there is an instrument holder that holds the different points that are used to indent the surface of the sample, and two different lenses that are used to set the sample to the correct position as well as analyse the indentation left by the tests. The stand is operated by the wheel in the base of the stand that can be turned to lower of raise the platform. The system is operated by an integrated computer and controlling software through the screen on the right side of the machine. The system has standardised test parameters saved in order for easy use of the machine by simply just choosing the correct test.

7 Experimental procedure

7.1 Job preparation

The jobs were designed with the idea in mind that those would give the best possible picture about how well the powder works in the machine (see Figure 17).

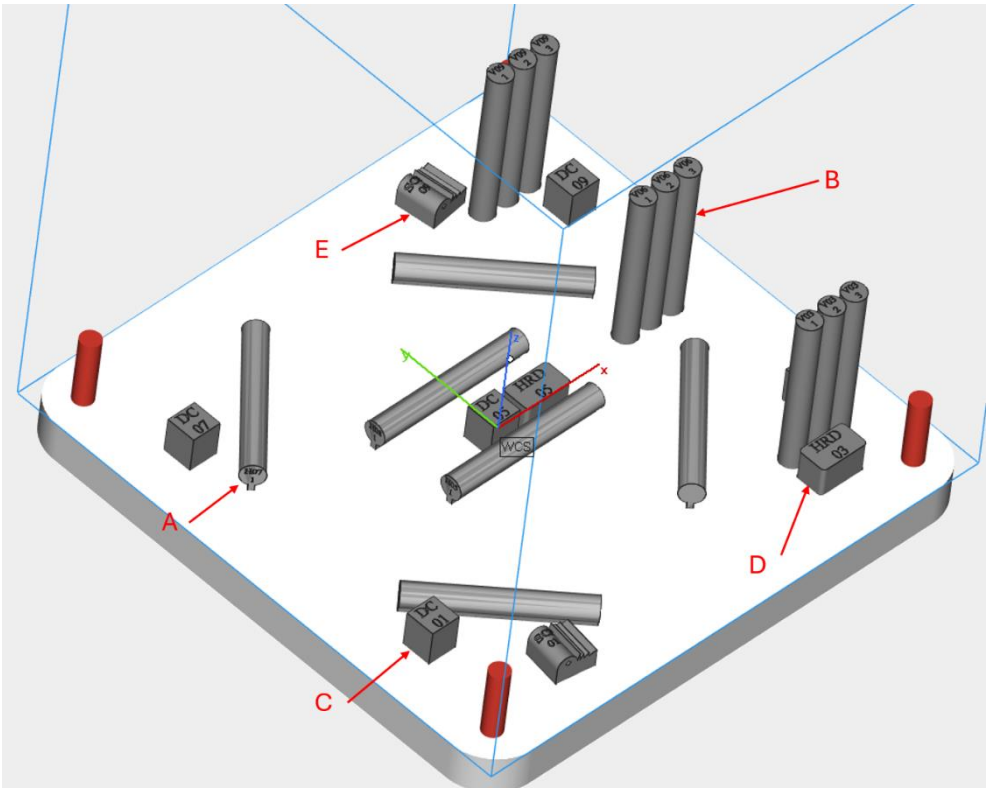

Figure 17. QC layout used in the AlSi10Mg jobs. A is horizontal tensile bar, B is vertical tensile bar, C is a density cube, D is the hardness test part and E is the porosity analysis part

First AlSi10Mg jobs were done using a quality control layout (Figure 17), which has density cubes, horizontal and vertical bars for tensile testing, two sub-contour porosity parts for porosity testing and two parts that are meant for hardness testing. This layout is low in load for the machine, and it gives a direct comparison to similar job layout used to create quality control data in EOS M290.

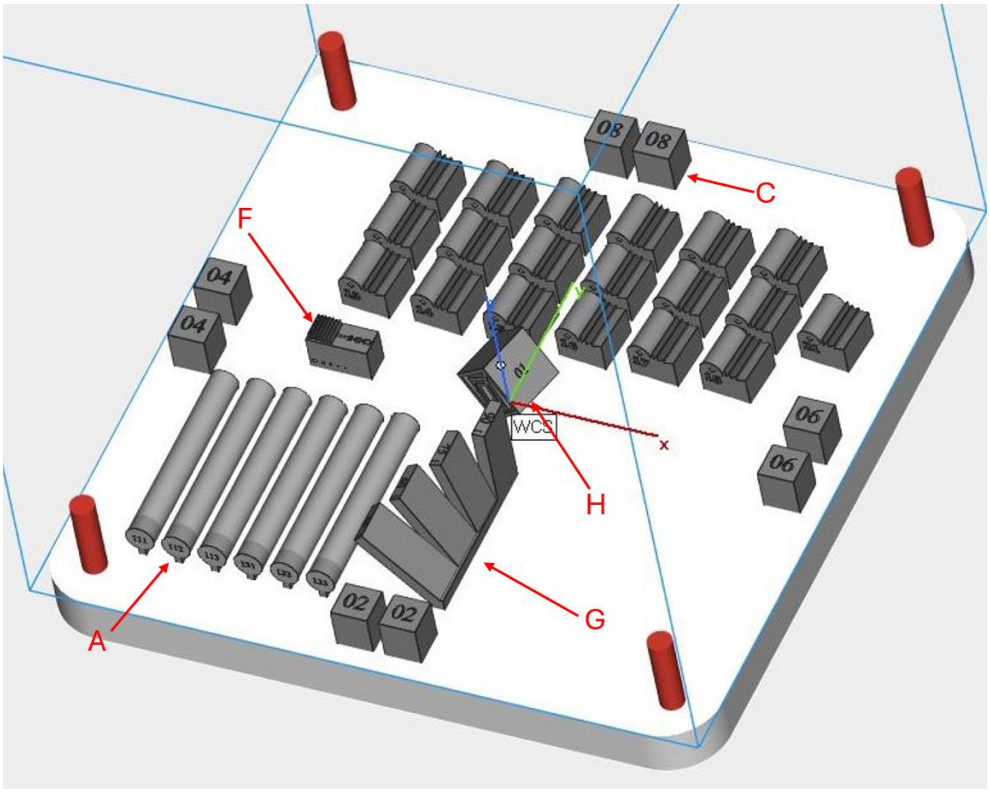

Figure 18. AlSi10Mg DOE job layout. A part is a horizontal tensile test bar, C is a density cube, F is the internal structures part, G is the surface roughness part and H is the optical microscopy and etching part

Second job that was prepared for aluminium, was a DOE layout (**Error! Reference source not found.**) that was made to test different parameters on the infill of the parts. 16 different combinations were made with four different laser powers, four different levels of heat input and four hatch distance settings along with three arbitrarily chosen parameter sets included for extra data. Eight density cubes were added to the layout with two cubes on each side of the building platform to characterize far ends of the slightly larger build area of SLM 280HL. Each pair was made using one parameter set on the other cube and second parameter set on the other. Two geometries were added to the center of the platform to test the downskin quality of the parts. Tensile bars were also added, half of which were heat treated after the job. Lastly some slats on different angles were added to study the surface roughness of the parts in different building angles.

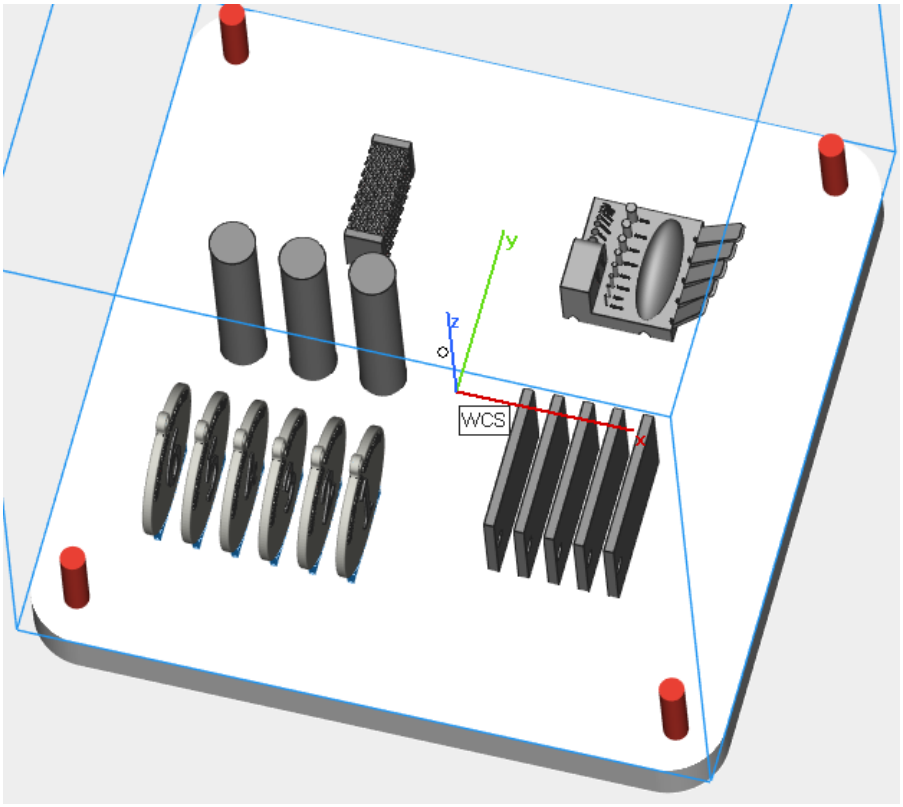

Figure 19. Buildability and corrosion test job

On the third layout that was made with aluminium (Figure 19), a buildability part was put in with different geometries such as a dome, slats in different angles to study the downskin and some holes and small diameter poles. The layout also has lattice part from which it's possible to study what the surfaces of such thin components looks like. Some corrosion testing parts were also put into the layout along with three bars and some medals for added load on the machine but the parts were not in the scope of the thesis to be tested.

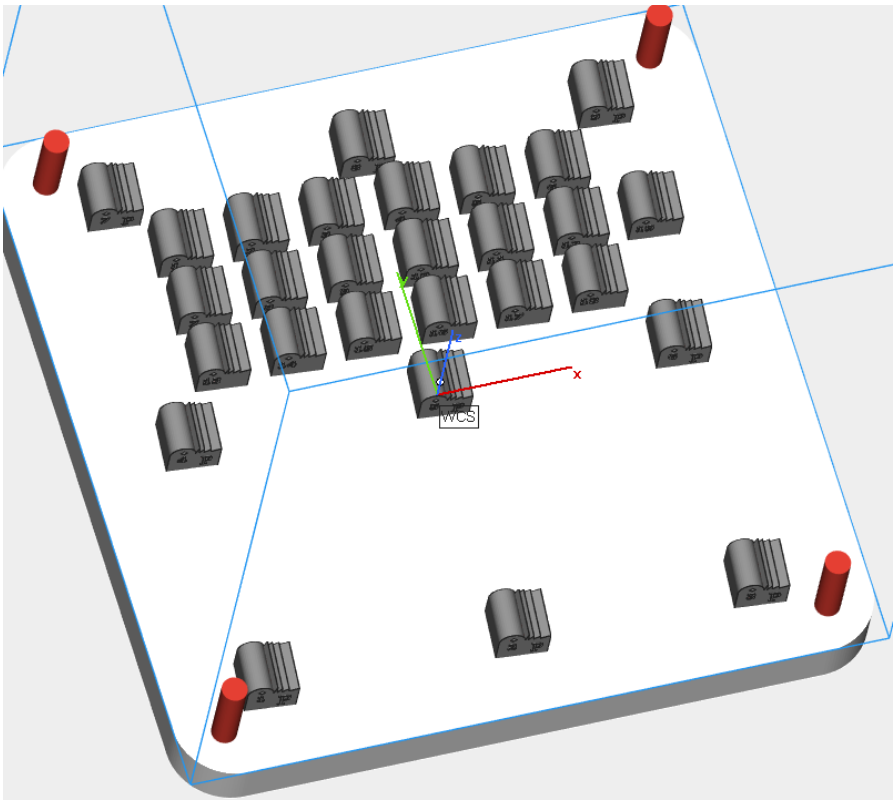

Figure 20. DOE job layout for MP1 and 316L consisting of only porosity test parts

The layout in Figure 20 was used to test different parameters in the process as well as to create the process parameters for 316L. The layout also has parts placed on the outside edges of the platform as well as one on the middle of the platform to study the effects of the placement of a part. This DOE layout consists only from the porosity test parts.

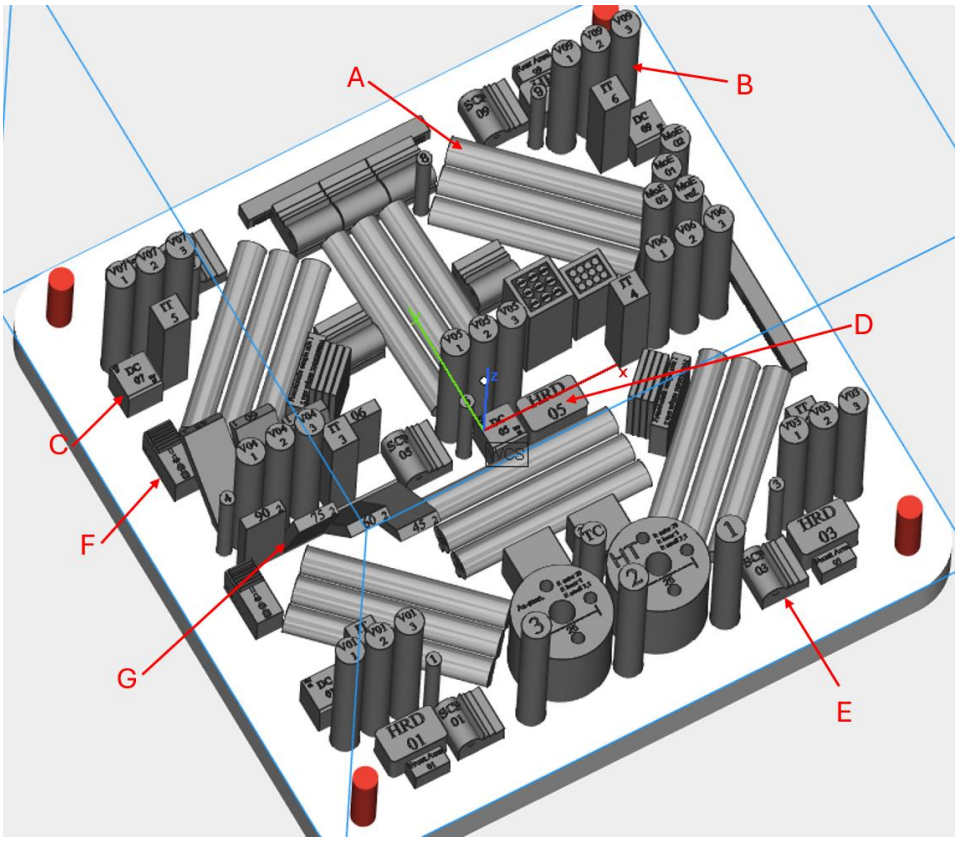

Figure 21. CV layout used with 316L and MP1. A is a horizontal tensile test bar, B is a vertical tensile test bar, C is a density cube, D is a hardness test part, E is a porosity test part, F is an internal structure part and G is a surface roughness part

The validation layout (CV) in **Error! Reference source not found.** was used to test the performance of the material in the given process. The platform has been filled with multiple different test parts, some of which were not tested because they were not in the scope of the thesis.

7.2 Sample manufacturing

7.2.1 Preparing the system

The samples were manufactured using the SLM 280HL. In the case of the SLM system, the process starts with sieving the powder so that there are no particles that are too big. Sieving is done after every built job so that the particle sizes remain constant and there are no particles

that are too big that would not melt properly during the next job. This is done because during the process, particles affected by the laser can form big particles that could disturb the process by not melting properly. At the start of the sieving process, the powder is transferred from plastic containers that the powder is stored in, to metallic containers that are about the same size. One metallic container is then transferred on to the sieving machine that has another similar container below the sieve to collect the sieved powder. When the containers are secured, before the start of the sieving, oxygen is removed from the sieving machine by flooding with argon gas to below 0,5 % oxygen level. This is in order to protect the powder from environmental effects like moisture pickup and oxidation. Then the sieving is started, and the sieve starts vibrating. The hatch that keeps the powder in the container can be opened letting the powder flow on to the sieve, and to the container below the sieve. After all the powder has gone through the sieve, the process can be stopped, and the containers can be taken out of the machine. After the sieving of a container is finished, the powder can be added to the machine by lifting the container above the machine and turned upside down and fixed into a feeding pipe with a metal clamp. Then the hatches are opened and the powder flows into the dispensing chamber of the machine. If the powder doesn't flow by itself, the container can be lightly hit with a plastic mallet to get the powder moving. When the container is empty, it can be taken off the machine and used in the next sieving round. The machine holds about 2-3 containers worth of powder, and one extra can be left on top of the machine if needed.

Preparing the machine starts by cleaning the building platform carrier and the platform itself. This is done by wiping them with a clean cloth and isopropanol alcohol to get all the dirt and grease off them. Then the platform is inserted on the carrier and secured with four screws, one in each corner of the platform. The platform is also leveled onto the correct height so that the recoater doesn't crash on the platform and to ensure the correct height of the first layer of powder. After the platform is secured, the lenses of the lasers are cleaned by also wiping them with isopropanol alcohol and wiping cloths, after which the lenses are checked by reflecting light off them to make sure no particles are left on them so that the laser beam does not hit them and cause particles to burn into the lenses or possibly reflecting the laser beam back to the optic system. Then from the controlling computer of the system, the saved job file is downloaded onto the machines controlling software from which you can control the job and see how long it's going to take to build the job. After that the platform heating and atmospheric build-up in the process chamber is started. The oxygen is removed from the process chamber by flushing it with argon gas until the oxygen level is below 0,10 %. When the oxygen level is below 0,10

% and the platform temperature has reached the pre-set temperature 150 °C in the cases of aluminium and cobalt-chrome and 80 °C in the case of stainless steel, the first layer of powder is spread on top of the building platform so that the layer of powder is see-through.

After all the preparations are finished, the process can be started from the machine's computer. The machine starts melting the powder layer by layer in the layout determined by the slicing software.

7.2.2 Post processing

After the job has finished in the SLM 280HL the post-processing can be started. First the building platform is allowed to cool down in peace so that the operator does not burn their hands. After the platform had cooled down, the platform is slightly lowered and the excess powder on the edges of the build chamber is vacuumed out so that it does not mix with the powder on the platform. Then the platform is raised step by step and the powder is swiped off the platform into the collector bin using a brush until the whole platform and the parts are cleared form most of the powder. Then the rest that cannot be brushed off is vacuumed out to get the platform free of any powder. After the platform is free of powder the platform is taken out of the machine.

Post processing is continued by marking the platform with the correct details and takin photographs of the build job so it can be studied later if needed. Then the parts were cut from the platform, cutting residue grinded off the parts and then put into a box.

7.2.3 Heat treatment of AlSi10Mg

Some of the AlSi10Mg tensile test parts were heat treated in order to alter the mechanical properties of the parts. Heat treatment lowers the tensile and yield strengths of the material while increasing the elongation, but the effects could be the other way around with different treating durations and temperatures. (Ghio & Cerri, 2022)

The first part of the heat treatment is a solution annealing to alter the microstructure and get rid of the layer-wise continuous structure in the cross-section caused by the process. Solution annealing also removes the internal stresses of the material caused by the manufacturing process. (Ghio & Cerri, 2022) The heat treatment was conducted by first heating the oven to 540 °C. When the oven was at the set temperature, the parts were inserted to the oven and kept there for half an hour starting from the moment that the temperature of the parts reached 530

°C. After 30 minutes soak time in high temperature, the parts were taken out of the oven and immediately submerged in water to quickly cool them down.

Second part of the heat treatment was a T6-aging. This means that the oven was heated to 170 degrees and when the temperature was reached, the parts were put in and kept there for 6 hours after the parts had reached 165 degrees. The temperature graphs in relation to time are shown as appendices.

The effect of the heat treatment could be altered by changing the temperature for the aging and also the time that the aging process lasts. Heat treatment could cause the yield and tensile strengths decrease and elongation to increase even more, or the effect can be completely the opposite where yield and tensile strengths increase and elongation decreases. (Rosenthal et al., 2018)

7.3 Sample analysis

7.3.1 Porosity analysis

The analysing of the porosity test parts started with cutting them in half and washing them thoroughly using an ultrasound cleaner to get any residue powder off the surface of the parts. Then the samples were made into round buttons using epoxy resin and left to set over night.

The dried-up buttons were then sanded and polished using a material specific recipe to get the sample surface levelled and completely smooth. The different steps in the polishing are shown in Table 6. First the aluminium samples were sanded using an 80-grit sandpaper for one minute and then on 320-grit sandpaper for 3 minutes to get the sample surface all flat. After the sandpaper the samples were polished using an MD-Largo polishing sheet for 7 minutes with diamond suspension liquid meant for this specific polishing sheet. After MD-Largo, MD-Mol was used for 8 minutes with a different diamond suspension automatically dropped onto the polishing sheet. Lastly on the rotating polisher an MD-Chem was used for 1:30 minutes with a third diamond suspension added manually this time. After all these steps, the samples were put into a vibration polisher for 1.5 hours to get a perfectly smooth surface to get the most accurate results from the porosity analysis.

Grinding and polishing of the 316L samples started with the 80-grit, 320-grit and 600-grit sandpapers. After that the polishing started with the MD-Largo for 8 minutes, then MD-DAC for 5 minutes, MD-Mol for 3 minutes, and MD-Nap for 3 minutes, after which the samples were ready to be analysed.

Table 6 Porosity analysis sample polishing recipes

	AlSi10Mg	316L	MP1
80-grit sandpaper	1 min	2 min	3 min
320-grit sandpaper	3 min	2 min	3 min
600-grit sandpaper	X	2 min	X
MD-Allegro	X	X	7 min
MD-Largo	7 min	8 min	X
MD-DAC	X	5 min	X
MD-MOL	8 min	3 min	20 min
MD-NAP	X	X	4 min
MD-Chem	1.5 min	X	X
Vibration polishing	1.5 h	X	1.5 h

The porosity analysis was done with an optical microscope using a 5x magnification lens. The software-controlled microscope is used to create a stitched image by automated stage movements to focus the microscope to each location on the sample surface, after which the picture could be modified to look good by cropping and tilting the image. On the sample surface, a rectangle was drawn to the bulk solid of the sample from which the analysis was done so that the contours were omitted from region of interest in the porosity analysis. Then an analysis tool is used from the control software of the microscope that recognises all the pores on the sample surface and highlights them. The analysis might also highlight some grooves on the surface or some dirt left even after the polishing, so the results are checked, and the wrongly highlighted areas are deleted from the analysis.

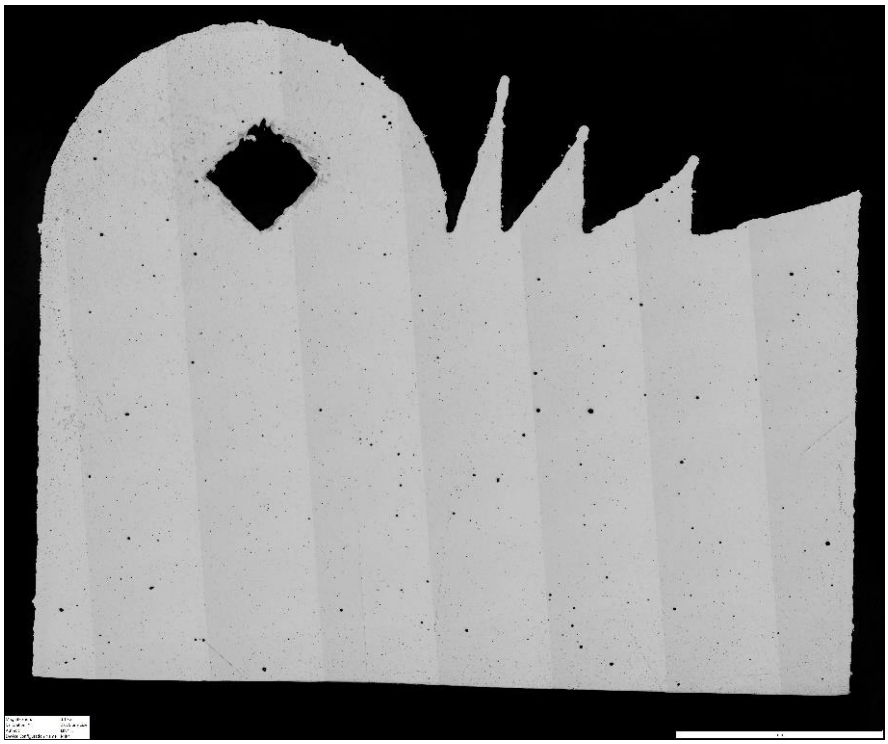

Figure 22. Porosity analysis sample image of AlSi10Mg

Cross-sections like the one on Figure 22 were analysed to receive the defect information of the parts. The sample shown in Figure 22 is made of AlSi10Mg.

7.3.2 Hardness analysis

Hardness testing was done using the EMCO-Test DuraVision machine. The hardness test parts were prepared by grinding the long edges so that the test surface would be flat and smooth. When the samples were prepped, they were put to the machine one by one. The aluminium parts were tested using the Brinell scale. Then 2.5 mm diameter tungsten sphere impedes the sample surface with a constant load of 62.5 kg, after which the systems software analyses the crater that was left on the surface and determines the hardness from the diameter of the crater. This procedure was repeated three times on different positions on the sample surface. To get a reliable result, enough material is left between each indentation so that deformation and working of the surface does not interfere with the next measurement.

316L and MP1 samples were tested using the Vickers hardness. HV10 test was used to measure the Vickers hardness. HV10 uses a load of 10 kg instead of the 62.5 kg in the Brinell hardness

tests and the point used in the test is the shape of a pyramid instead of a ball like in the Brinell tests.

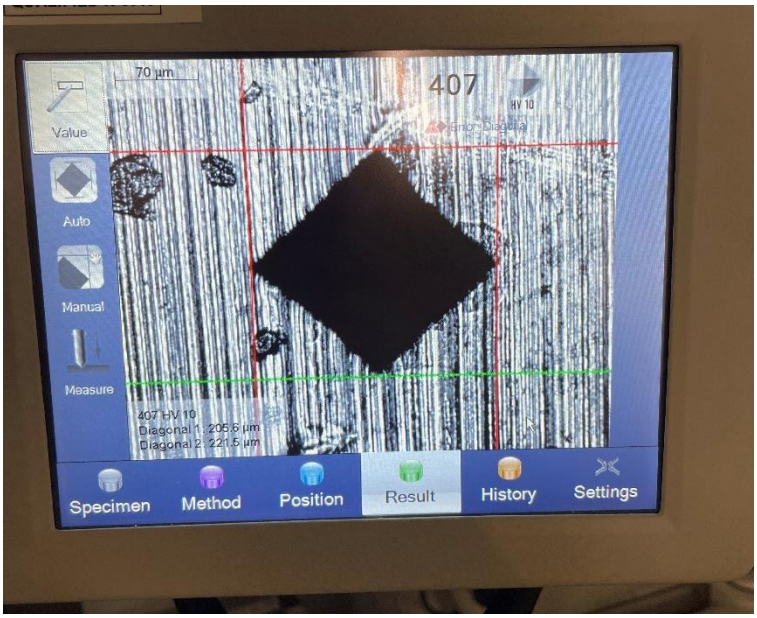

Figure 23. Hardness analysis method

Figure 23 shows the image that the system uses to measure the hardness. The lines are automatically set to the edges of the indentation and can also be manually moved. The software calculates the hardness based off of the size of the indentation.

7.3.3 Surface roughness analysis

Surface roughness analysis was done using the Alicona InfiniteFocus G5 focus variation measuring instrument (Figure 15). The parts were put on a surface under the objective and an overview picture from each sample was taken. When the samples are set on to the surface, controlling software of the Alicona scanner is used to set the correct positions on x-, y- and z-axis, between of which the scan of the sample surface is taken. Setting the range on the z-axis was important to get all of the individual peaks to be visible on the analysis. After the range was set, the machine took images from the whole test area at various focus distances and made a 3D-model from the surface. From the model, the whole area was analysed to get the *Sa* values of the surfaces. Also, the *Ra* values were determined using the Alicona by taking an image from a smaller area of the sample and then drawing a line in a zigzag formation on the sample in the length of 40 mm from which the program determined the profile of the line and calculated the

wanted values. Examples of the area for the *Sa* and profile for the *Ra* measurements are shown in Figure 24.

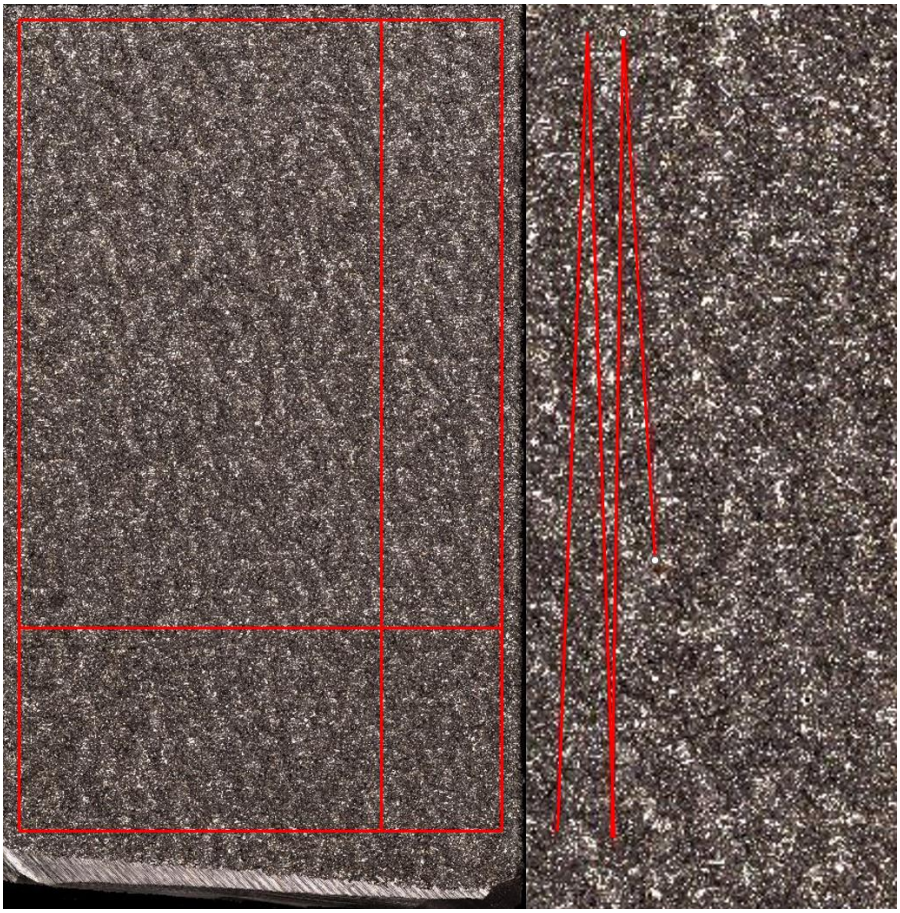

Figure 24 *Sa* and *Ra* measurement area and profile

7.3.4 Density analysis

Densities of the materials were determined using the Archimedean method. The cube was grinded smooth on all sides so there would be no air bubbles trapped on the samples surfaces to disturb the measurements.

The measurement setup was put on top of a scale. A cup of water and a holder for the samples with one surface in air and one surface submerged in the water cup. The scale was the zeroed and an analysis program started on the scale. The temperature of the water was measured and inserted into the program to calculate the density of the water. Then the cube was put on the measurement surface that was above the water surface and the weight of the cube was saved in the program. Then the cube was measured on the surface submerged in water and the program calculated the density of the material from the results.

Figure 25. Density analysis setup

7.3.5 Tensile tests

Tensile tests were performed to measure the tensile strength and the elongation of the parts. Horizontal and vertical bars were tested. A part of the horizontal bars was heat treated prior to tensile testing. Tensile tests were outsourced to DEKRA and Element and were executed using the test specifications supplied by EOS, that are according to the ISO 6892 specification. In the cases of AlSi10Mg and MP1, the gauge length (length of the neck area) was 5D (5 times the diameter of the neck area) according to annex D of ISO 6892. When testing the 316L samples, gauge length 4D was used to enable comparison to long term data created by EOS.

7.3.6 Optical microscopy

Parts were also studied using an optical microscope. Figure 26 shows the pictures taken from the DOE job of AlSi10Mg

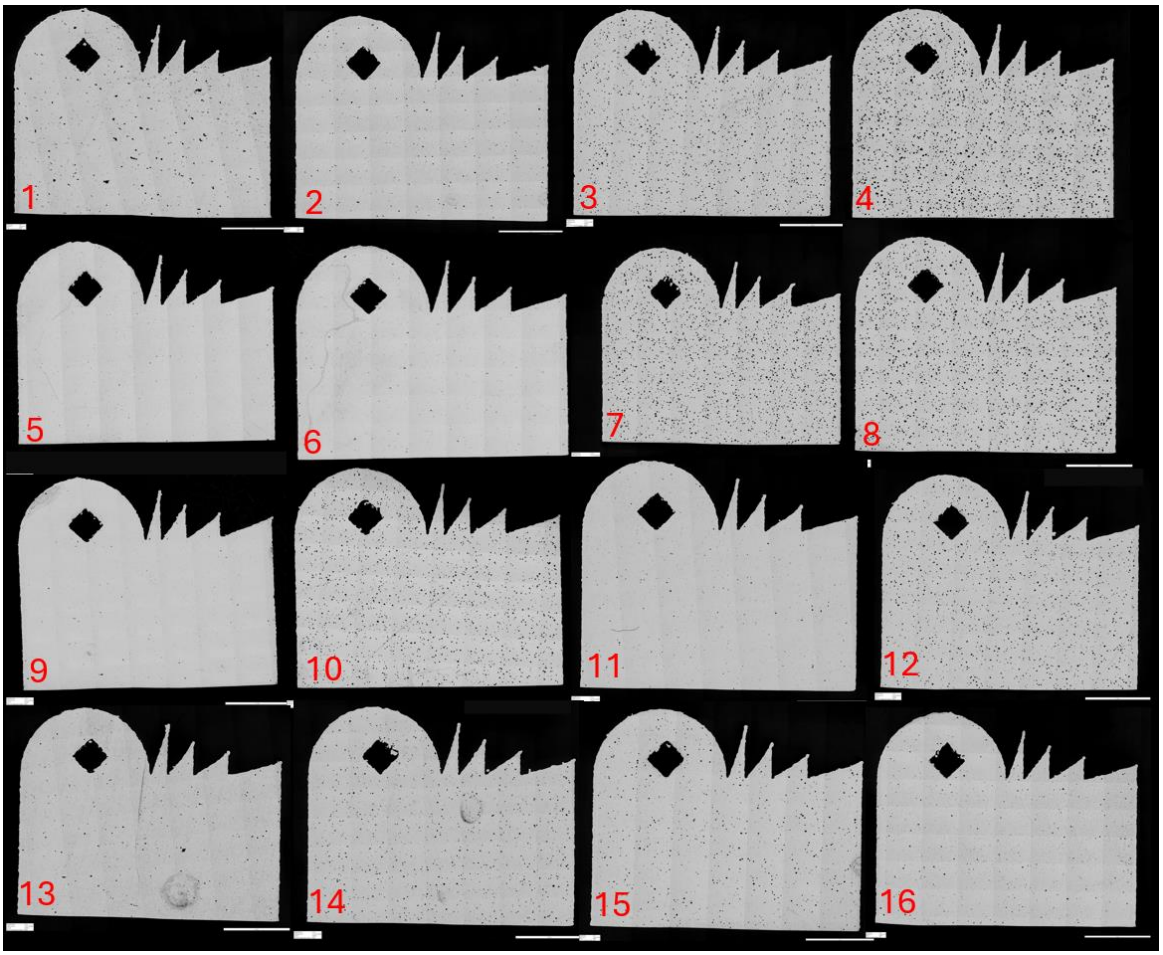

Figure 26. Example of optical microscopy on AlSi10Mg DOE design

Each of the pictures in Figure 26 were analysed individually to get the results of the porosities for ach parameter set.

Some AlSi10Mg parts were etched using a Kellers etch HF reagent at Dekra Turku, to get a better phase contrast and more detailed view to the microstructural features, such as melt pool boundaries. The etching however was not successful as the final surface seemed to have etched too much, which makes the analysing of the surface quite difficult. The resulted images from the etched parts are shown in Figure 27.

Figure 27. Etched AlSi10Mg parts. EOS material on the left and SLM material on the right

7.3.7 Taguchi analysis

Porosity results from the DOE job were analysed using the Taguchi analysis method.

The main contribution of the Taguchi design is the ability to reduce combinations tested to find the most suitable parameter combination with most effect to optimized function with least variation. Taguchi methodology enables for example reducing variability and increasing robustness of a process by providing ranking and significance of different parameters to the measured signal as well as determining the optimum control parameters with least noise caused by uncontrollable error parameters.

The expected outcome from the Taguchi analysis is a product that does not get affected by changing conditions, such as in the case of this thesis, the placement on the platform. (Karna, n.d.)

The results of the Taguchi analysis are:

- Significance of the parameters to the received results
- Determining the optimal level of factors by conducting a main effects analysis
- Execution of an analysis of factor contribution rate
- Confirmation of the experiment

8 Results and discussion

8.1 AlSi10Mg

AlSi10Mg jobs started by doing the QC layout jobs, followed by the DOE jobs. SLM powder was used first, followed by EOS powder before moving on to the next job layout.

Table 7 AlSi10mg porosity analysis report from the DOE job

	Defect-%		> 100 µm (pcs.)	
Parameter set	SLM powder	EOS powder	SLM powder	EOS powder
1	1.052	1.070	137	139
2	0.501	0.459	14	18
3	3.259	2.485	271	170
4	6.485	5.074	759	582
5	0.263	0.183	6	5
6	0.313	0.214	9	6
7	4.913	3.749	518	348
8	4.753	4.144	479	492
9	0.217	0.140	1	3
10	3.013	2.322	185	136
11	0.423	0.321	24	18
12	2.765	2.180	223	164
13	0.646	0.392	17	16
14	1.321	1.174	62	45
15	1.092	0.973	44	43
16	0.612	0.609	35	20
17	0.258	0.225	2	6
18	0.233	0.253	6	5
19	0.123	0.135	2	1

The porosity results of AlSi10Mg DOE job are presented in Table 7. The deviation in the results showcases that the parameter window was wide enough to have comparison of powders made also on less optimal process parameter areas. If one powder would be more robust against the process changes, it would be shown in the comparison of the results. When the results are analysed, the EOS powder yields better results compared to the SLM powder when the parameters are clearly faulty. Even on the better suited parameters the EOS powder yields better or at least roughly similar results when compared to the SLM powder, which suggests that the

powder behaviour of EOS powder is equal or even better than the behaviour of the SLM powder.

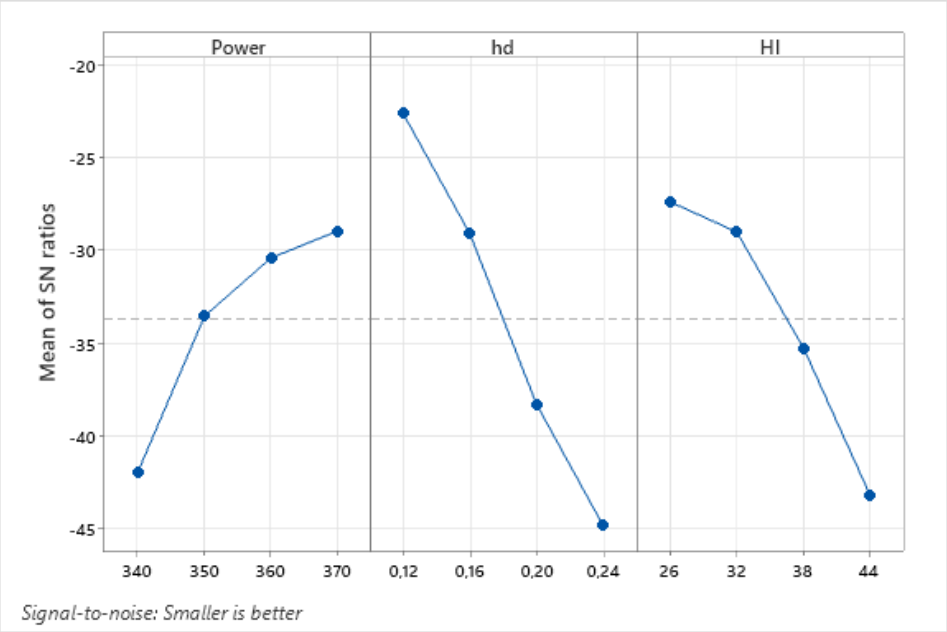

Figure 28. Taguchi analysis of AlSi10Mg parameter variables. Power is the laser power, hd means hatch distance and HI means heat input. SN ratio means the effect on the results.

Taguchi analysis was conducted from the porosity results of the DOE job. The results of the Taguchi analysis are shown in Figure 28. In the diagrams the closer to zero the result is, the better. So therefore, the best outcomes come with a power of 370, hatch distance of 0.12 and a heat input of 26. These results seem plausible when discussed with the experts at EOS Oy. In the Taguchi methodology, the best combination is not necessarily included in the test matrix. In this case the combination was not in the matrix, so the results should be confirmed by testing the parameters by manufacturing more parts with these parameters.

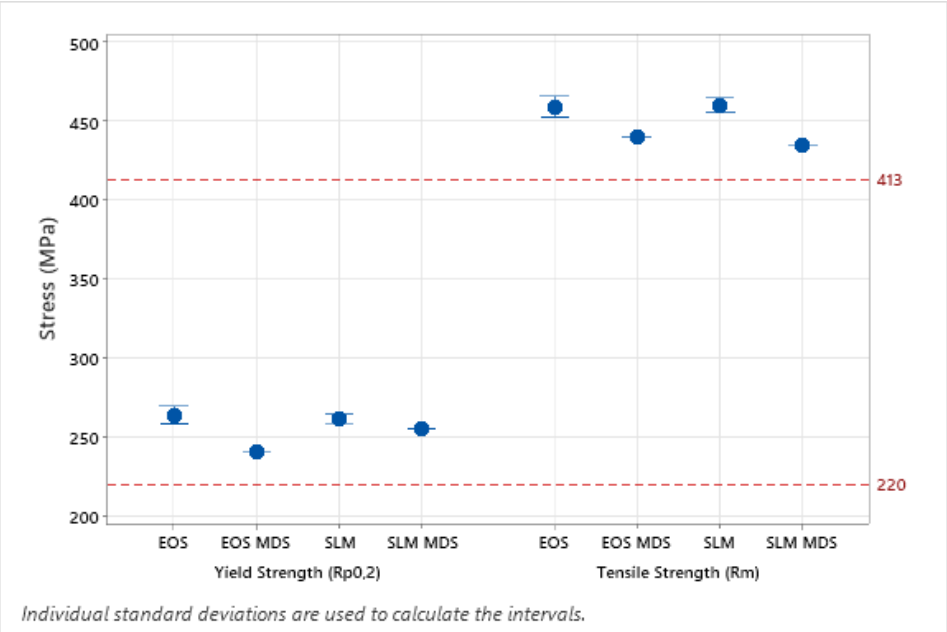

Figure 29. Yield and tensile strengths of vertically built AlSi10Mg parts compared to the MDS values and the material standards indicated with the red lines

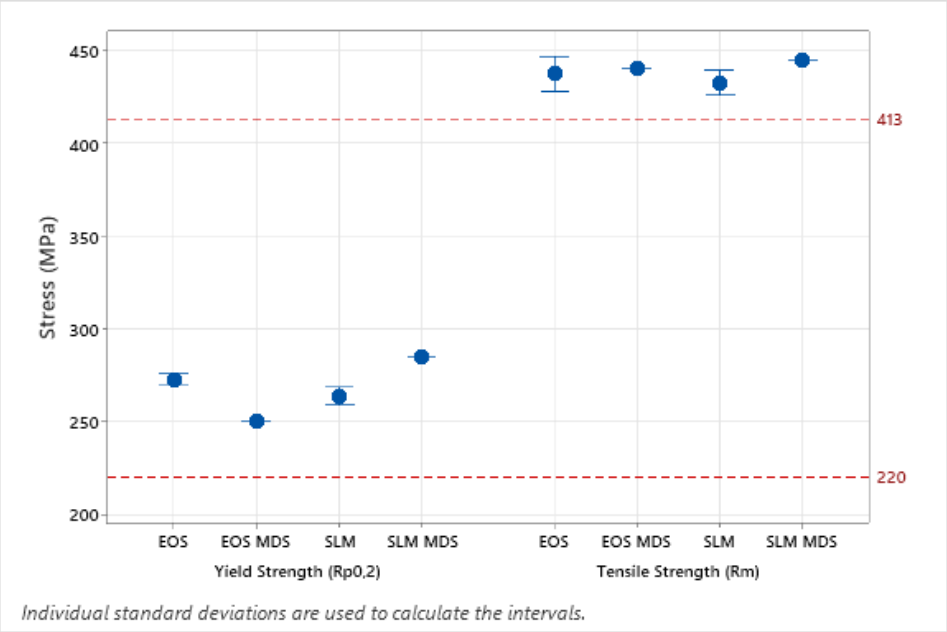

Figure 30. Yield and tensile strengths of horizontally built AlSi10Mg parts compared to the MDS values and the material standards indicated with the red lines

Figure 29 and Figure 30 shows that both materials have similar performance when it comes to the proof and tensile strengths. This can be said as the data points labelled EOS and SLM are on the same level with each other. In the vertical parts, both materials exceed the MDS values of both manufacturers. The horizontal parts meet the MDS values of EOS, but the SLM MDS values are higher than the actual results that was achieved with either material. These results could possibly be further improved by optimizing the process parameters for the EOS powder, but considering the fact the EOS powder performed similarly than the SLM powder, or even better, proves that the EOS powder works well in the SLM 280HL as is.

All of the yield and tensile test results regarding the as-manufactured AlSi10Mg parts are well above the minimum requirements of over 220 MPa of yield strength and 413 MPa of tensile strength, that are in the standard specifications of the material ASTM F3318-18. (F42 Committee, n.d.)

The scrap rate of the material was also calculated from these builds. The achieved scrap rate for the AlSi10Mg jobs were 37.52 % for the EOS powder and 32.46 % for the SLM powder. These results are high compared to normal scrap rates achieved with either materials and are most likely caused by lack of experience of using the SLM 280HL system.

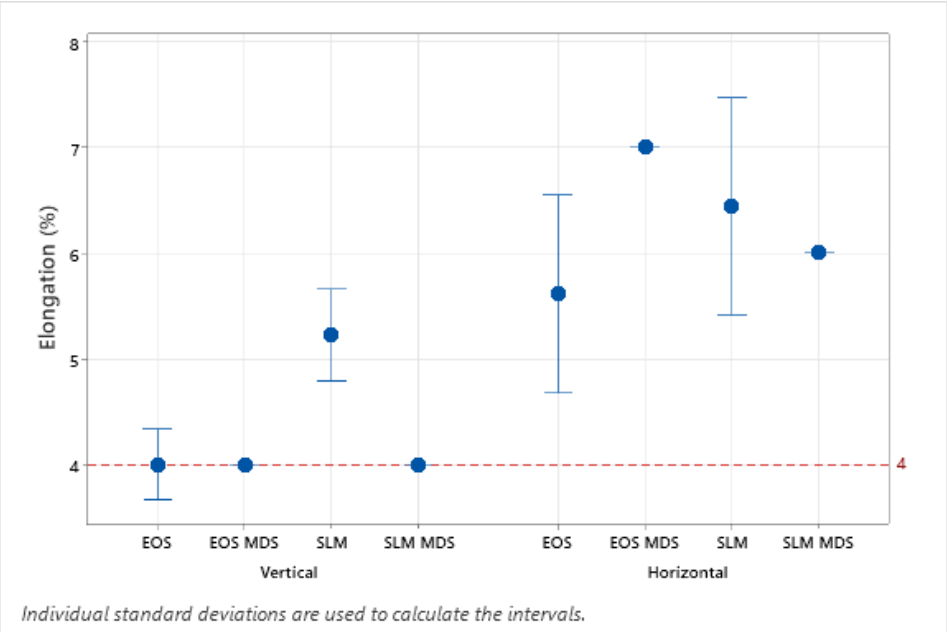

Figure 31. Elongation of AlSi10Mg parts compared to the MDS values and the material standard indicated with the red line

The measured elongation of both vertical and horizontal tensile test parts are shown in Figure 31. Results show that on the vertical parts, both materials perform as well as the MDS values or better as the results are on on the same level as the MDS values, whereas in the horizontal parts the results are a bit under the MDS values of EOS, but the materials perform similarly when compared to each other. The elongation results are also on par or above the requirement of the material standard that is 4% of elongation.

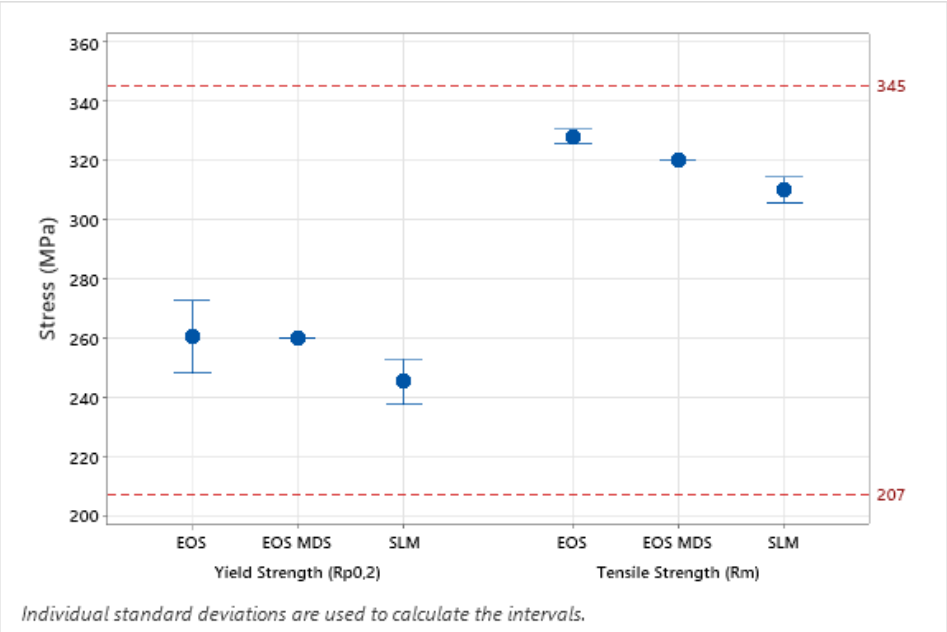

Figure 32. Yield and tensile strengths of heat treated horizontal AlSi10Mg parts compared to the MDS value of EOS and the material standards indicated with the red lines

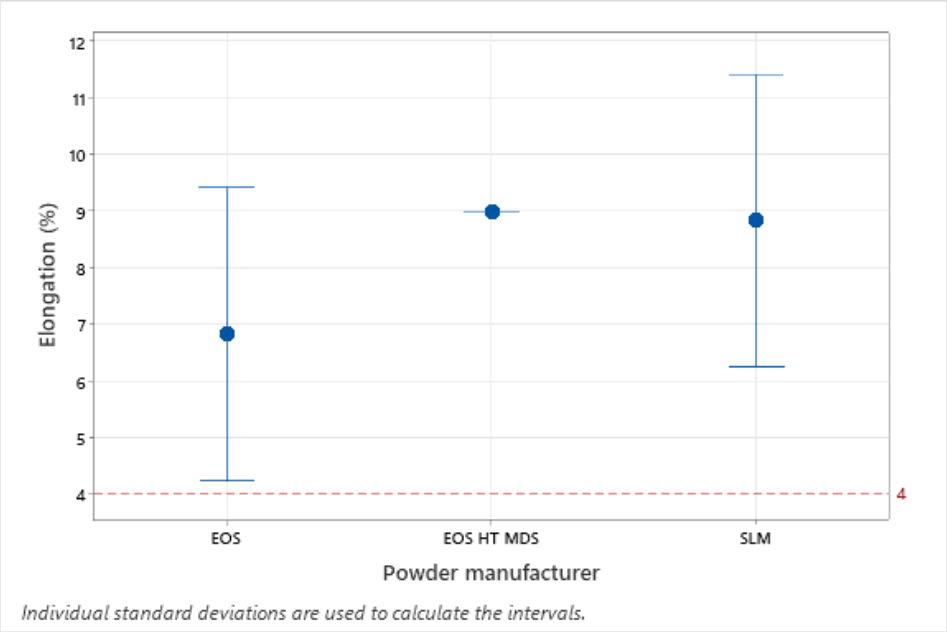

Figure 33. Elongation of heat treated horizontal AlSi10Mg parts compared to the MDS value of EOS and the material standard indicated with the red line

Figure 32 and Figure 33 show that the yield and tensile strengths and elongations are similar with both materials and when compared to the MDS value of EOS, as the deviation in the results overlap each other and the MDS value. These properties can be fine-tuned by optimizing the

heat treatment process as the effect is slightly different because of the different process parameters in the process itself compared to EOS parameters. The fine tuning of heat treatment process is proposed to be tested in future research. The results were not compared to MDS values of SLM as the material data sheet has no values for heat treated AlSi10Mg. These results could be made more precise with a larger number of samples as the test batch was small in this test.

Surface roughness measurements were tested using the Alicona InfiniteFocus G5 and these results can be seen in Figure 34. The results show that the EOS powder behaves better in the lowest building angle. Figure 34 shows that in the 45-degree building angle, the part made with EOS powder has a lower surface roughness than the one made with SLM powder. This might be due to the smaller particle sizes in the powder that provide a denser powder bed, that supports the structures being built in lower angles better. In 60-, 75- and 90-degree building angles, the results are closer to each other as the data almost on the same level with each other. These are made on the SLM parameters, and the results might be different if the surface parameters were modified slightly to suit the EOS powder better.

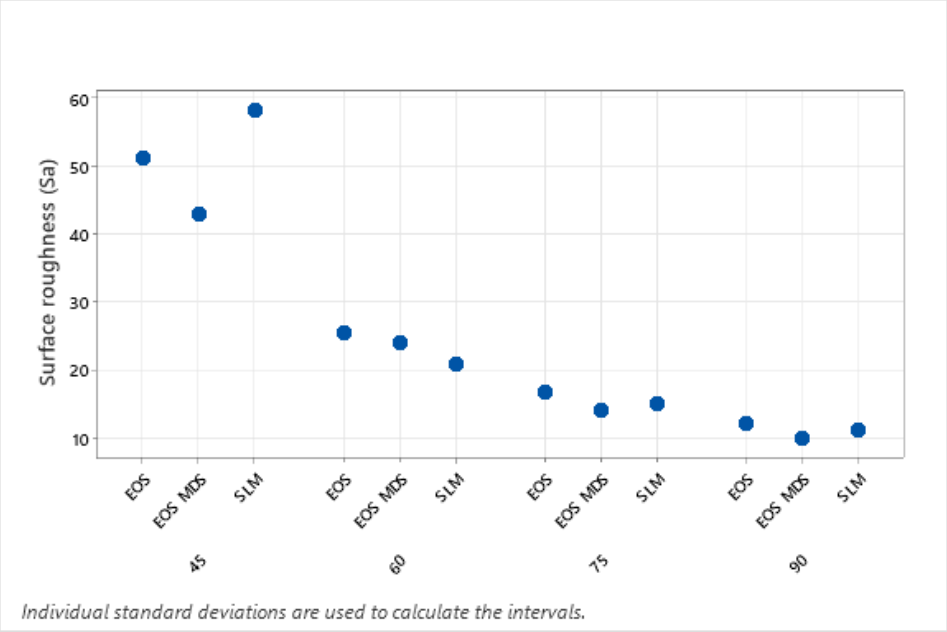

Figure 34. AlSi10Mg surface roughness in different building angles compared to the EOS MDS values

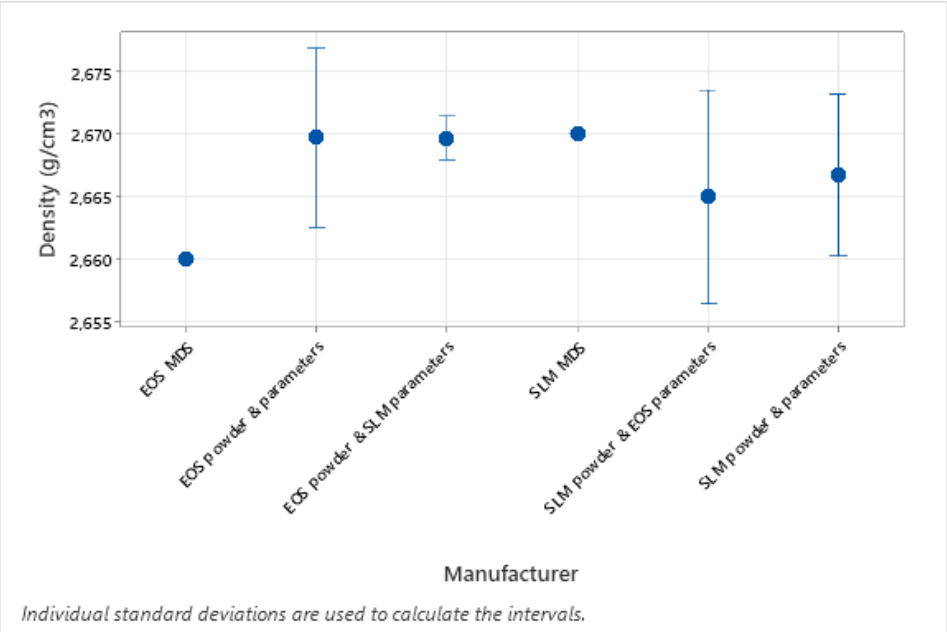

Figure 35. AlSi10Mg densities compared to the MDS values

The parts for the density testing were made with multiple combinations of parameters and materials. There were parts made with EOS powder utilizing EOS parameters as well as SLM parameters. There also were parts made with SLM powder with EOS and SLM parameters. The results from this experiment are shown in Figure 35. The results show that all the densities are on the same level with each other as well as with the MDS values of both companies. The results show that the process parameters have little to no effect on the density of the material if the parameters are suitable for the material processing. This further proves that the performance of both powders is similar in the SLM 280HL printer.

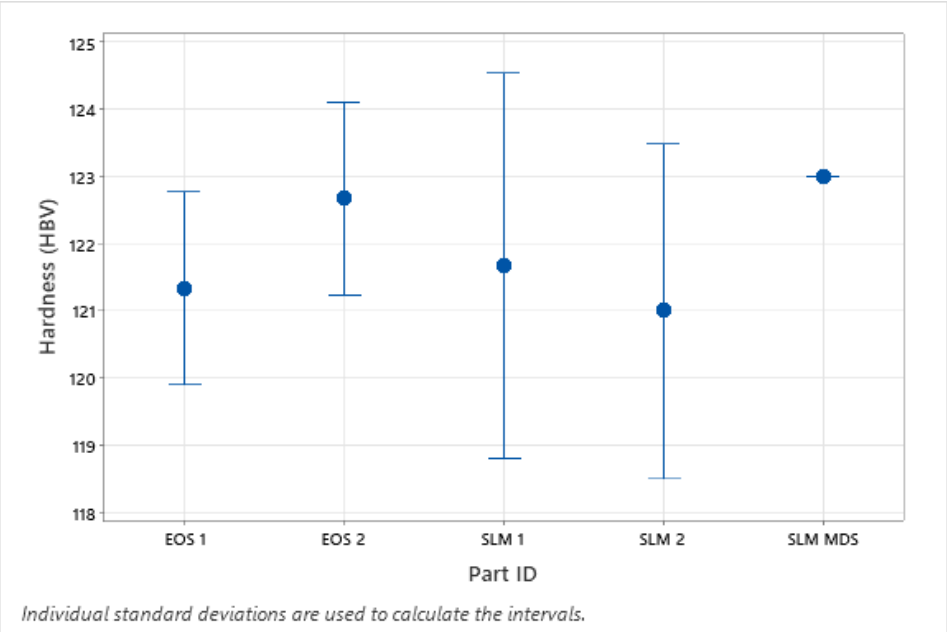

Figure 36. AlSi10Mg hardness compared to the SLM MDS value

Hardness values received from the experiments are shown in Figure 36. In Figure 36, the EOS 1 and EOS 2 are two similar parts that have been differentiated in the results to show the two samples and the SLM parts are dine the same way. All the samples have been manufactured using the SLM parameters. The figure shows two parts made with EOS powder and SLM powder, all of which were tested three times each. The results show that the hardness of both sets of parts are similar and on the same level as the MDS value presented in the data sheet of SLM.

8.2 MP1

In the case of MP1, there was no SLM supplied powder available, so the experiments were done only using EOS supplied powder. The experiments on MP1 started by doing a DOE job with placement dependent parts also in the job with both EOS and SLM parameters. The DOE job was made using a 60 µm layer thickness. After this a CV job was done using the SLM 60 µm process.

Table 8 MP1 DOE parameters

Laser power (W)	Hatch distance (mm)	Heat input (J/mm^3)
280	0.1	40

310	0.11	50
340	0.12	60
370	0.13	70

Table 8 shows the process parameter variables that were used in the DOE job of MP1.

Table 9 MP1 porosity analysis results from the DOE job

Parameter set	Defect-%	>100 µm (pcs.)
1	0.235	12
2	0.040	1
3	0.036	2
4	0.072	1
5	0.041	0
6	0.028	0
7	0.036	0
8	0.037	1
9	0.039	2
10	0.022	0
11	0.033	0
12	0.023	0
13	0.050	3
14	0.024	0
15	0.066	0
16	0.061	0
17	0.059	0
18	0.030	0

From the porosity analysis results on Table 9, it can be observed that there is some variation in the results between different parameter sets. Parameter set 10 has the lowest amount of porosity with 0.022 defect-% and the highest amount of porosity is in the part made with parameter set 1. The variation is not as big as seen with AlSi10Mg for example as the parameter variation in the DOE was narrower.

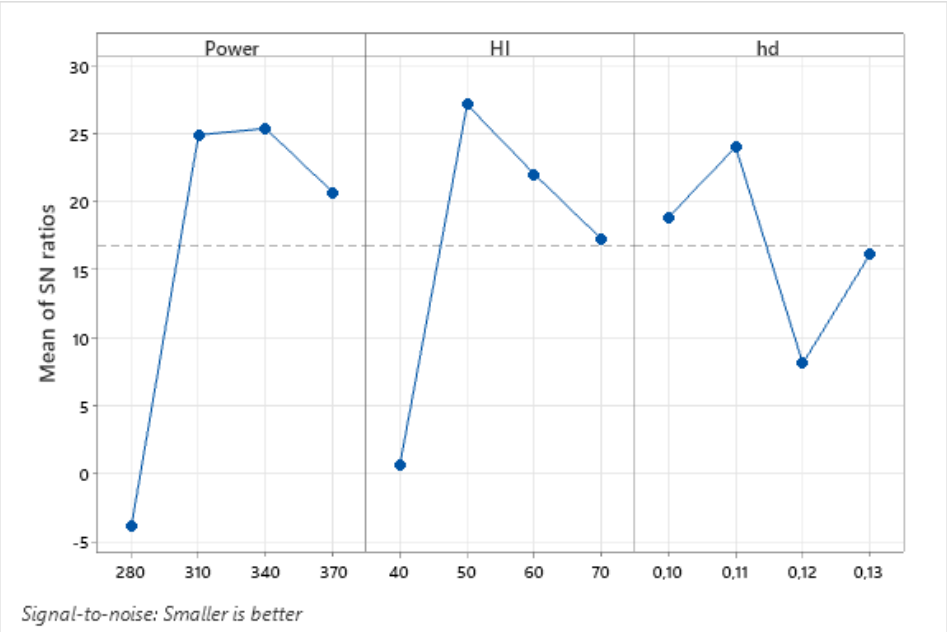

Figure 37. Taguchi analysis of MP1 parameter variables

The Taguchi analysis results in Figure 37 show that the optimal parameter configuration from these variables are laser power of 340 W, HI of 50 J/mm^3 and a hatch distance of 0.11 µm. When the results were viewed with the material experts at EOS, The results seemed plausible considering the existing parameters.

Table 10 MP1 position dependent porosity analysis results

Sample ID	Defect-%	>100 µm (pcs.)
1P	0.044	1
1EP	0.232	16
2P	0.032	0
2EP	0.063	0
3P	0.024	0
3EP	0.050	2
4P	0.037	0
4EP	0.106	6
5P	0.045	0
5EP	0.060	4
6P	0.023	0
6EP	0.033	0

7P	0.043	2
7EP	0.201	16
8P	0.026	0
8EP	0.040	0
9P	0.042	0
9EP	0.026	0

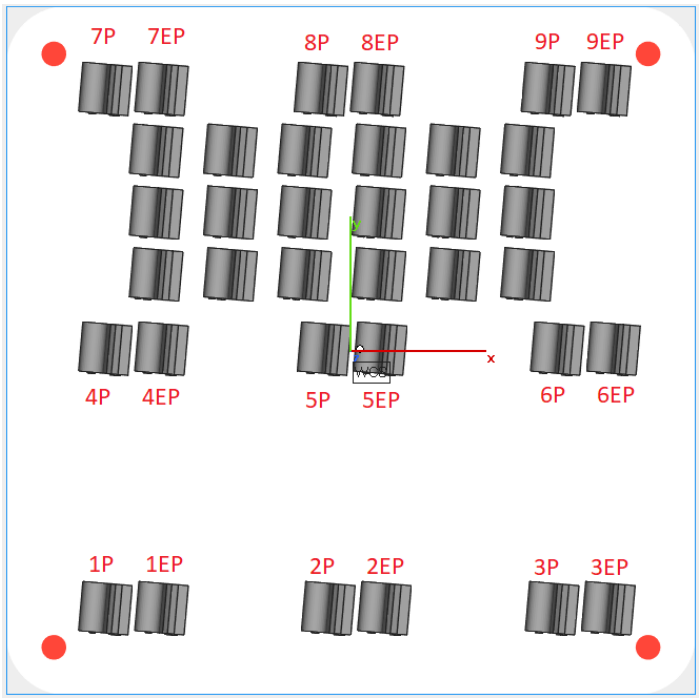

Figure 38. MP1 position dependend job part placements

The position dependent results of the MP1 DOE job are seen in Table 10 and the positioning of each part is seen in Figure 38. The samples marked with xP were made using the SLM CoCr28Mo6 60 µm process and the ones named xEP are made using the 60 µm MP1 process of EOS, that is still in development. From the results we can see that the deviation in the defect-% is small in the parts made with the SLM parameters, whereas the parts with the EOS parameters are more affected by the position of the part. This effect is caused by the lower intensity of the laser because of the higher angle of the laser beam when going to the further edge of the platform (Tolvanen, 2024) and the oversized particles from the parts being built upstream of them are left onto the further parts, causing the energy to not be enough to properly

melt the oversized particles. This effect could be mitigated by optimizing the parameters for EOS powder, but this was not in the scope of the thesis.

Table 11 Porosity results from the MP1 CV job

Sample ID	Defect-%	>100 µm (pcs.)
1	0.045	1
2	0.049	1
3	0.040	1
4	0.036	1
5	0.041	0
01	0.053	1
03	0.027	0
05	0.045	0
07	0.045	0
09	0.020	0

The porosity results from the CV job can be seen in Table 11. The defect-% in all of the parts is low and the number of large pores is minimal. MP1 has a habit of creating small cracks in the microstructure of the bulk material and this causes there to show some large pores as this is calculated by measuring the distance between the absolute furthest points from one another on the defect.

The scrap rate for the MP1 was calculated to be 28.5 %. This is calculated based on only the one CV job, so the scrap rate could differ from the result achieved by making multiple builds. The scrap rate could also be improved if the parameters would be optimised for the EOS powder, as the parameters now used are developed for the cobalt-chrome material of SLM.

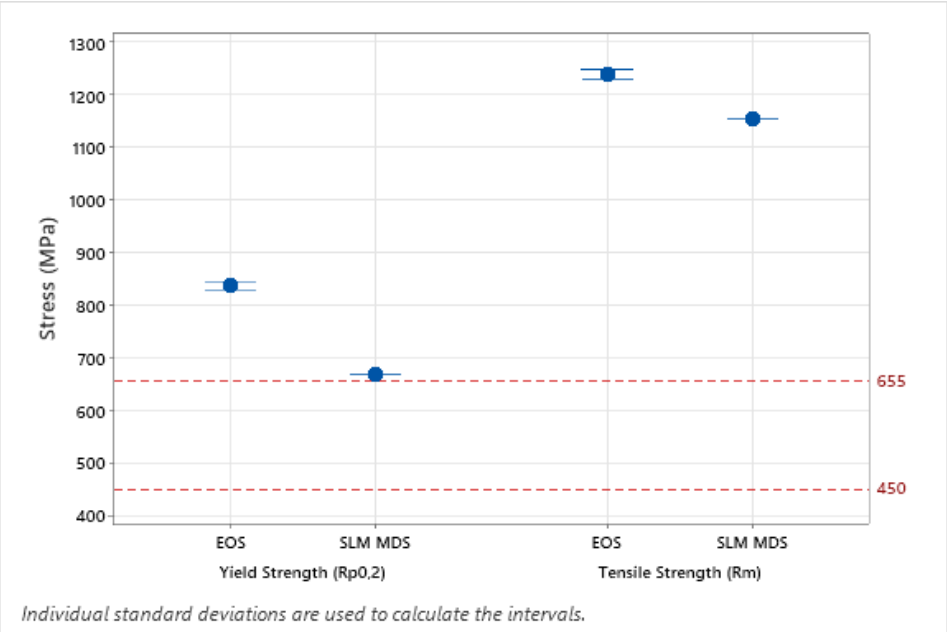

Figure 39. Yield and tensile strength of vertical MP1 parts compared to the SLM MDS values and the material standards indicated with the red lines

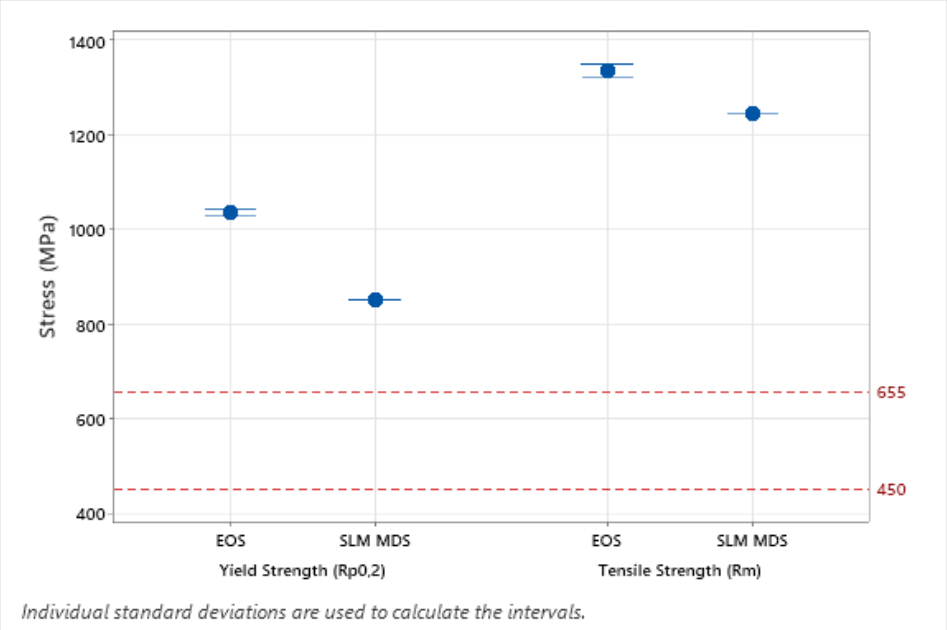

Figure 40. Yield and tensile strength of horizontal MP1 parts compared to the SLM MDS values and the material standards indicated with the red lines

From Figure 39 and Figure 40, it can be seen that the yield and tensile strength results received from the MP1 CV job are looking great when compared to the MDS values of SLM. The results are also well above the minimum requirements set by the material standard ASTM F213-17

(ASTM International, n.d.). So by looking at these results it can be said that there is no problem with using the EOS MP1 in SLM 280HL, considering the tensile properties.

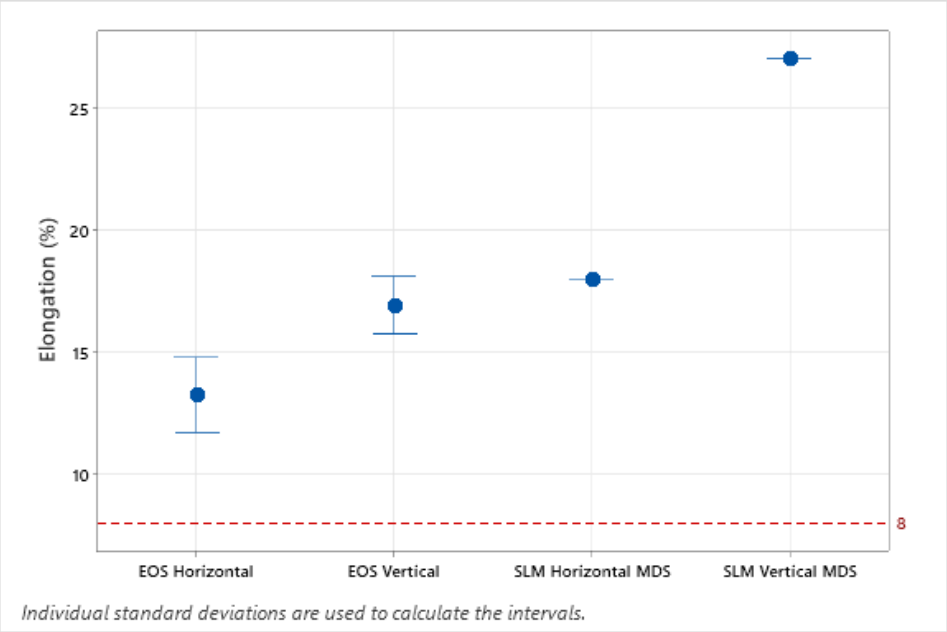

Figure 41. Elongation of MP1 parts compared to the SLM MDS values and the material standard indicated with the red line

When the results in Figure 41 are analysed, it can be seen that the elongations that we were able to produce are not as high as the elongations mentioned in the SLM MDS. The elongations with EOS powder are however well above the standard minimum that is 8%. The lower elongations might be because of the process parameters that are not optimized for the EOS powder, and therefore the conditions for the process might not be ideal and could well be improved.

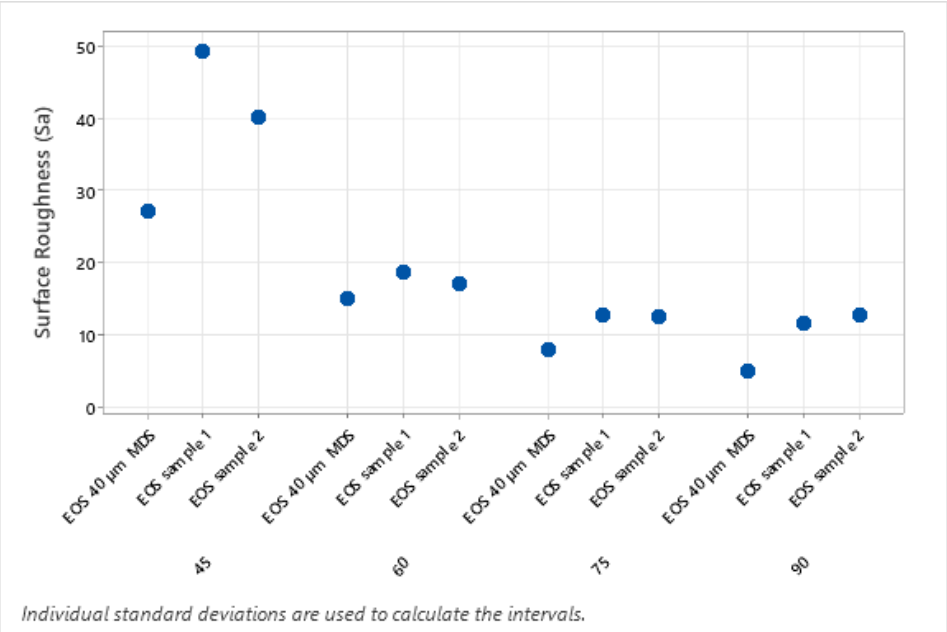

Figure 42. Surface roughness of MP1 parts in different building angles compared to the EOS MDS value for the 40 µm process

The surface roughness results of EOS MP1 are shown in Figure 42. From the results we can see that the surface roughness of the parts does not meet the same level as with the EOS MDS values for the 40 µm process. This is most likely due to the combination of the facts that the process is meant for SLM powder that is slightly different from the EOS powder and that this is a 60 µm process, where the surface is usually rougher than on the lower layer thicknesses. The results are compared to the 40 µm values from the EOS MDS as there are no values for the 60 µm process in the MDS.

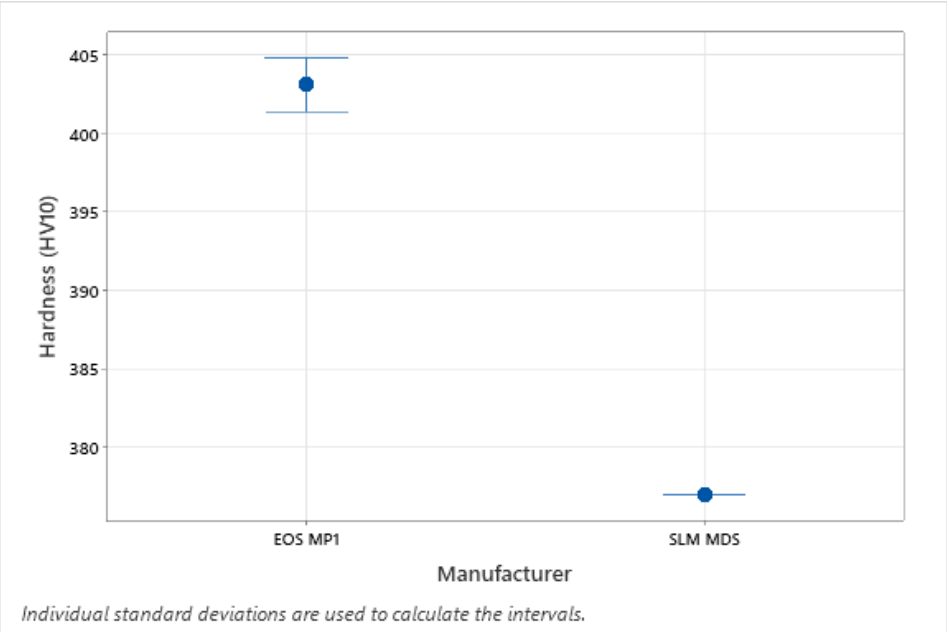

Figure 43. Vickers hardness of MP1 samples compared to SLM MDS value

Hardness values are shown in Figure 43. The figure shows that the hardness of the test samples is higher than the reference value from the MDS of SLM. This shows that the EOS powder performs well in the SLM 280HL in regard to the hardness of the final product.

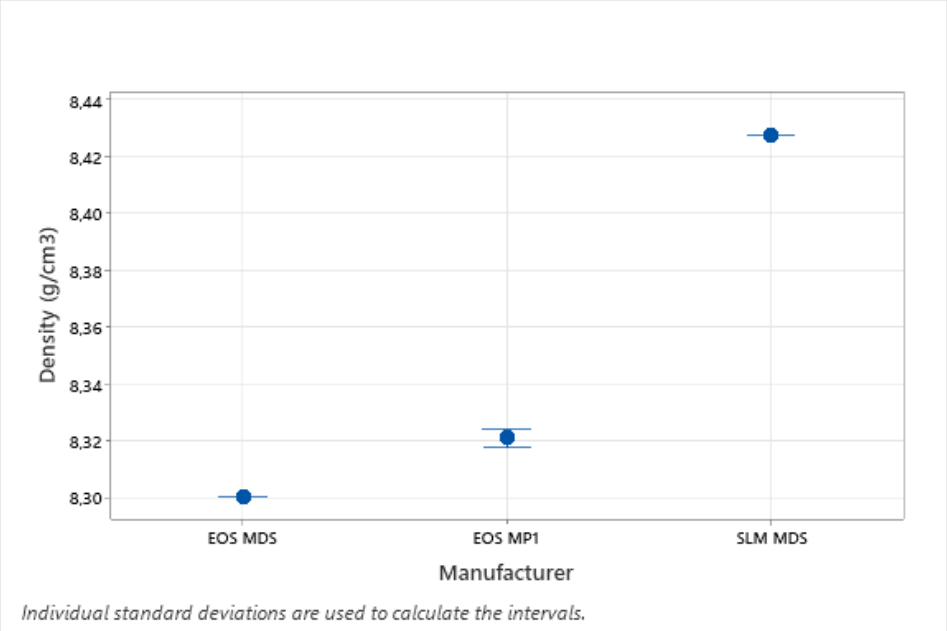

Figure 44. Density of MP1 samples compared to the MDS values

Figure 44 shows the density results of MP1 samples. The results show that the samples are on the similar level as the EOS material data sheet shows. The MDS value of SLM however is

higher than the received result with the EOS powder. This is most likely due to the fact that the material in the MDS of SLM has a slightly different chemical composition as the MP1 of EOS.

8.3 316L

With the 316L powder, a DOE job was conducted because there were no process parameters available from SLM. The different parameters used in the DOE job were planned with the help of EOS experts. These parameters are shown in Table 12.

Table 12 316L DOE parameters

Power (W)	Hatch distance (mm)	Heat input (J/mm^3)
290	0.1	30
320	0.12	36
350	0.14	43
370	0.16	50

These parameters were used to create different parameter sets that each of which was used to build a porosity analysis part to examine how well the parameters work. Also, two 80 µm layer thickness parameter sets from EOS were used as well as one parameter set with 40 µm layer thickness. The porosity results from the DOE job are shown in Table 13.

Table 13 316L porosity analysis report from the DOE job

Parameter set	Defect-%	>100 µm (pcs.)
1	2.749	311
2	0.243	15
3	0.201	6
4	1.008	6
5	0.068	1
6	0.324	23
7	0.261	2
8	0.296	9
9	0.086	6
10	0.074	0
11	0.828	121

12	0.295	36
13	0.072	3
14	0.116	6
15	0.439	42
16	1.837	355
17	0.124	1
18	0.117	3
19	0.033	0

A Taguchi analysis was conducted from the results of the DOE job and the resulting diagrams from this analysis are shown in Figure 45.

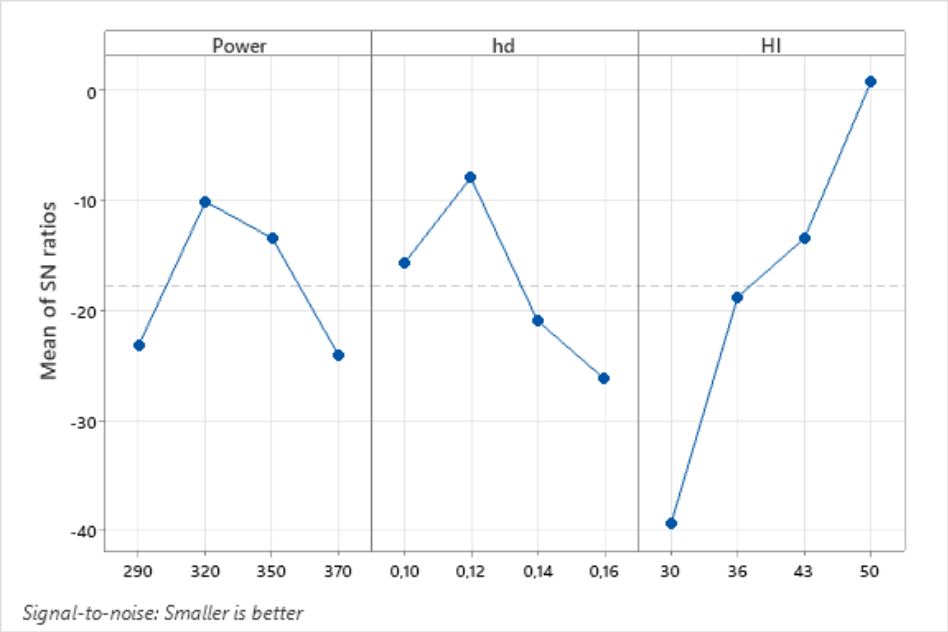

Figure 45. Taguchi analysis of 316L parameter variables

In the diagrams the closer the point is to zero on the y-axis, the better the parameter is. From the diagrams we can thus see that the most optimal parameters are power of 320 watts, hatch distance of 0.12 µm and heat input of 50 J/mm^3. These parameters were then put into use to build the CV job.

Table 14 316L position dependent porosity analysis results

Sample ID	Defect-%	>100 µm (pcs.)
1P	0.250	18
2P	0.196	15
3P	0.083	0
4P	0.289	11
5P	0.205	15
6P	0.094	2
7P	0.288	21
8P	0.174	8
9P	0.083	0

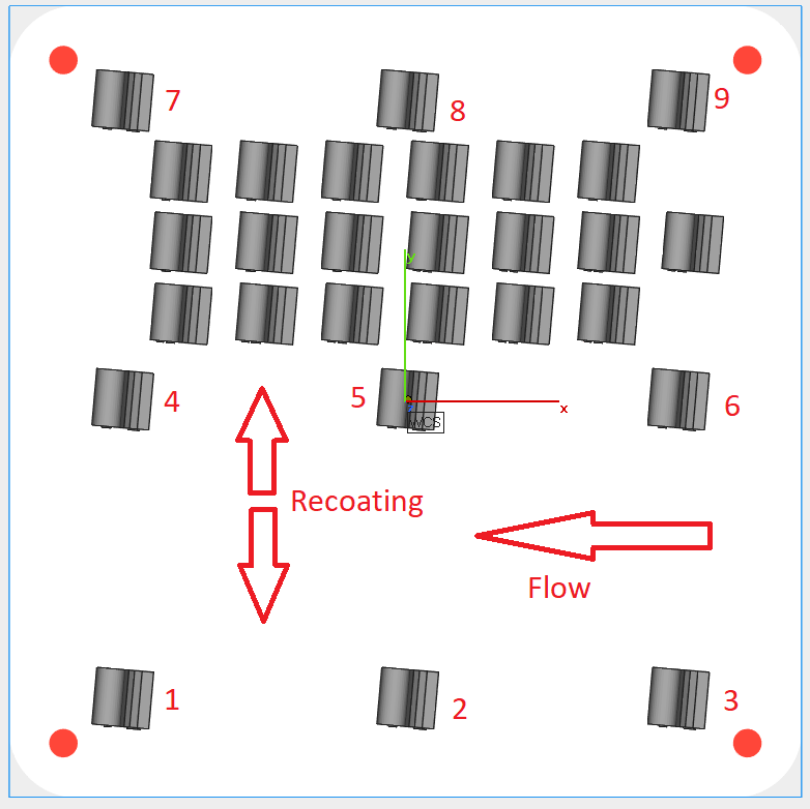

Figure 46. Position dependent job part placement

In Table 14 are the results from the position dependent study and from Figure 46, the placement of each part can be seen relative to the recoating and gas flow directions. The results indicate that the positioning of the parts on the platform of SLM 280 HL has drastic effects on the build

quality of the parts. On the side of the platform that the gas flow is coming from, the porosity results are much better than the results on the middle and on the far side of the platform. This most likely happens because the further the position is from the flow source, the more irregular the flow is. Also, the further away the position is, the more the spatters from the parts being built upstream of the flow will land on them. Oversized particles do not behave in the process as the correct sized powder would.

The parameters that were acquired from the DOE job were used to build the CV job with 316L. The contour parameters of EOS were brought to the job to get the best possible surfaces on the parts.

Table 15 Porosity test results from the 316L CV job

Sample ID	Defect-%	>100 µm (pcs.)
1	0.131	2
2	0.125	0
3	0.095	0
4	0.099	1
5	0.119	1
01	0.090	0
03	0.074	0
05	0.090	0
07	0.121	0
09	0.090	0

Table 15 shows the porosity results from the 316L CV job. From the table it can be seen that the porosities are looking good when compared to the MDS of EOS that promises defect-% of below 0.2 %. Further looking into the porosity results, the placement of the parts does not seem to be having much effect on the defect-% with these parameters. However, there were no porosity test parts in the outermost edges of the build platform so it cannot be said if it would have more drastic effects on the outside edges.

Scrap rate achieved with the 80 µm process developed for the 316L was calculated to be 27.9%. This result is calculated based on only the CV job, so the scrap rate could differ from the results achieved here, if more jobs are made with the parameters. The parts were manufactured with the parameters developed in this thesis, meaning that the scrap rate could possibly be improved by further optimising the parameters.

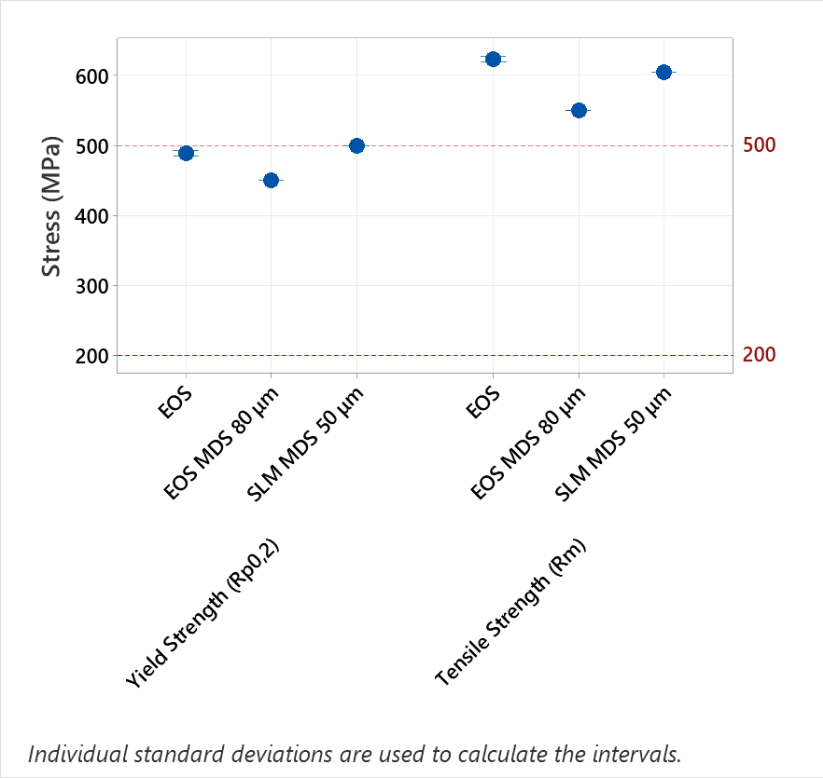

Figure 47. Yield and tensile strengths of vertically built 316L parts compared to the MDS values and the material standards indicated with the red lines

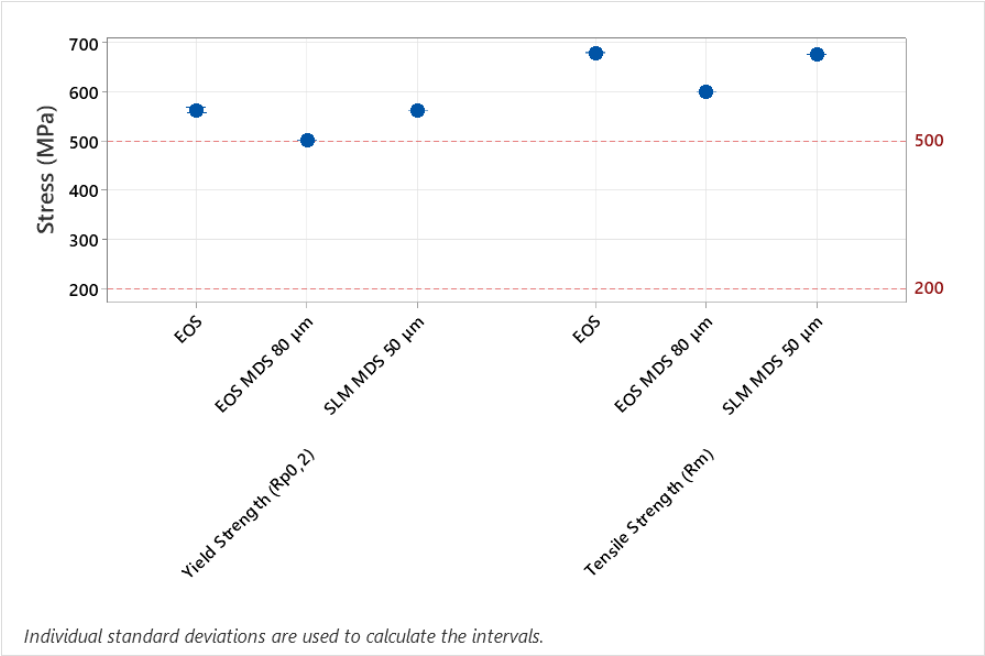

Figure 48. Yield and tensile strength of horizontally built 316L parts compared to the MDS values and the material standards indicated with the red lines

From Figure 47 and Figure 48 we can see the yield and tensile strength results of vertically and horizontally built parts. We can see that the results are excellent when compared to the MDS values of EOS and MDS values of SLM 50 µm process. The results are also well above the minimum requirements set by the material standard DIN EN 10088-3. These result prove that in regards to the yield and tensile strengths of the EOS 316L, the powder is ready to be used in the SLM 280HL. Properties of the material could however be modified still if the parameters are further developed and optimized as this was the result of only one test parameter, even though the parameters were discussed with the material experts at EOS.

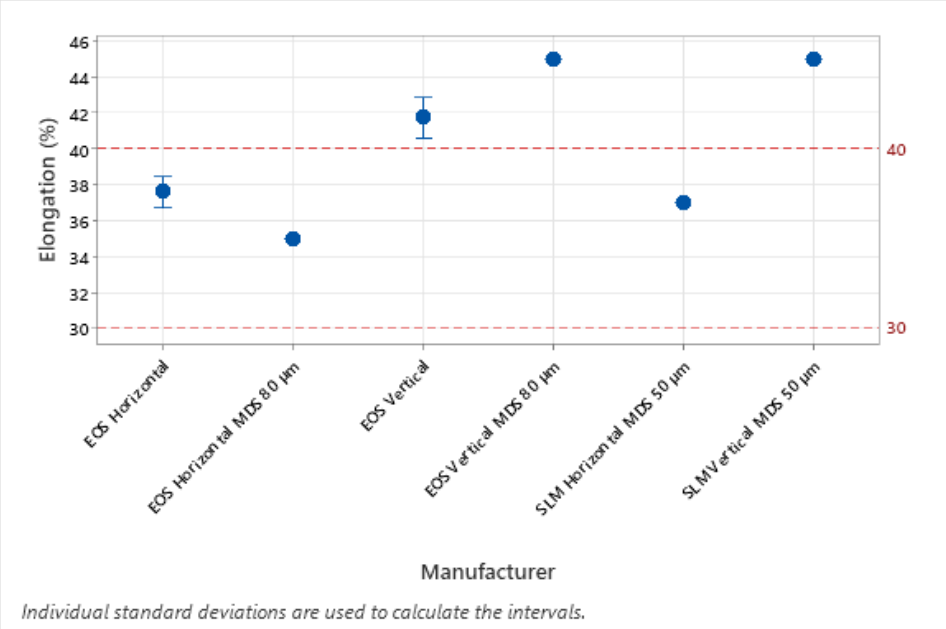

Figure 49. Elongation of 316L parts compared to the EOS MDS values and the material standards indicated with the red lines

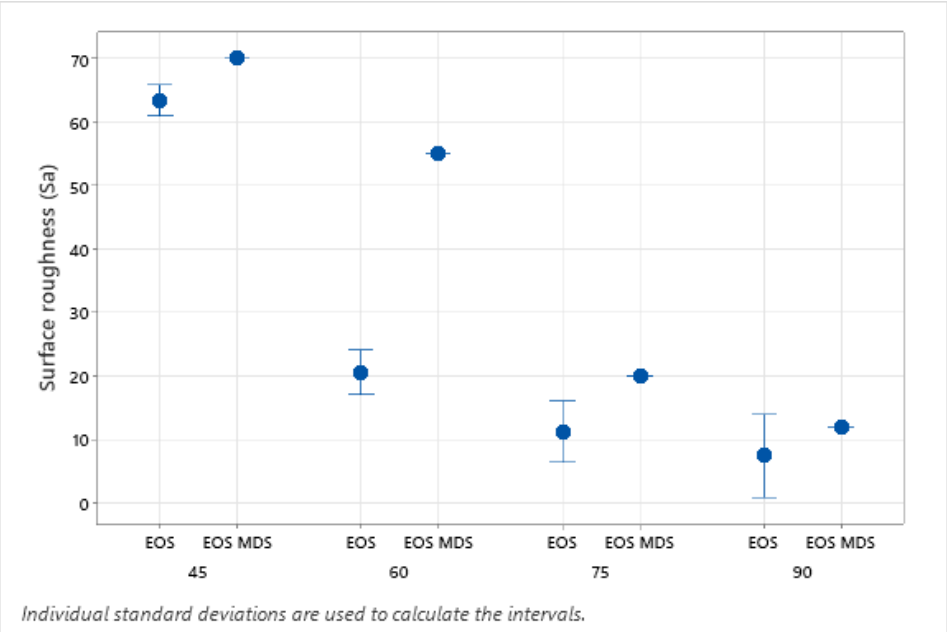

Figure 50. Surface roughness of 316L parts in different building angles compared to the EOS MDS values

The surface roughness results are shown in Figure 50. The results show that the surface roughness's are looking good when compared to the MDS values. This comes as no surprise as the parts were built using the surface parameters from EOS process. The surface roughness could however possibly be made even better by optimizing the surface parameters for this specific process to the SLM machine.

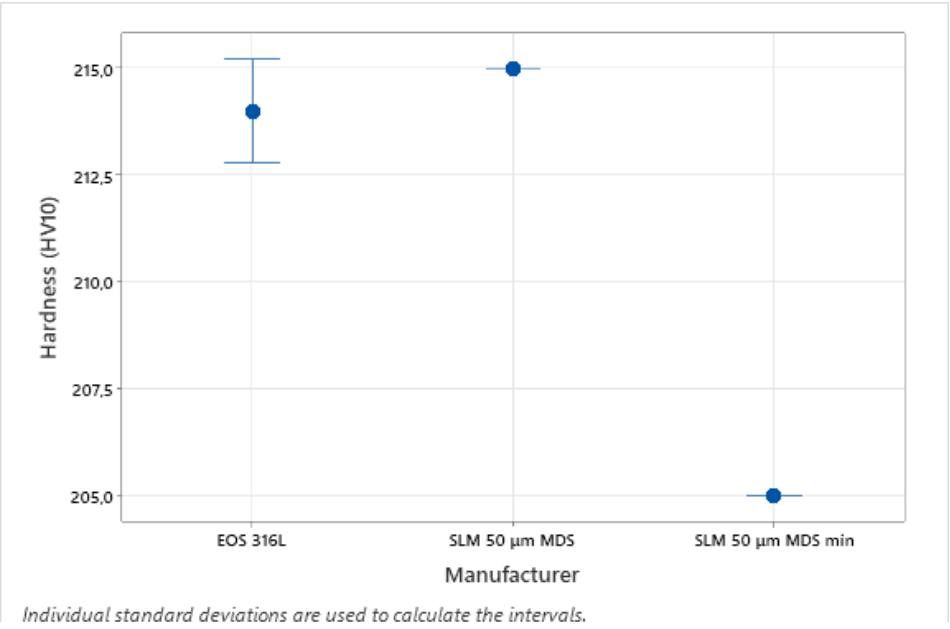

Figure 51 Hardness values of 316L sample compared to SLM MDS values

The Vickers hardness results in Figure 51, show that the hardness of the parts are on the same level as the hardness of 316L shown in the MDS of SLM. The hardness values are also well above the minimum value of 205, that has a 95% confidence level according to the MDS. Meaning that at least 95% of samples from a batch are above this level of hardness.

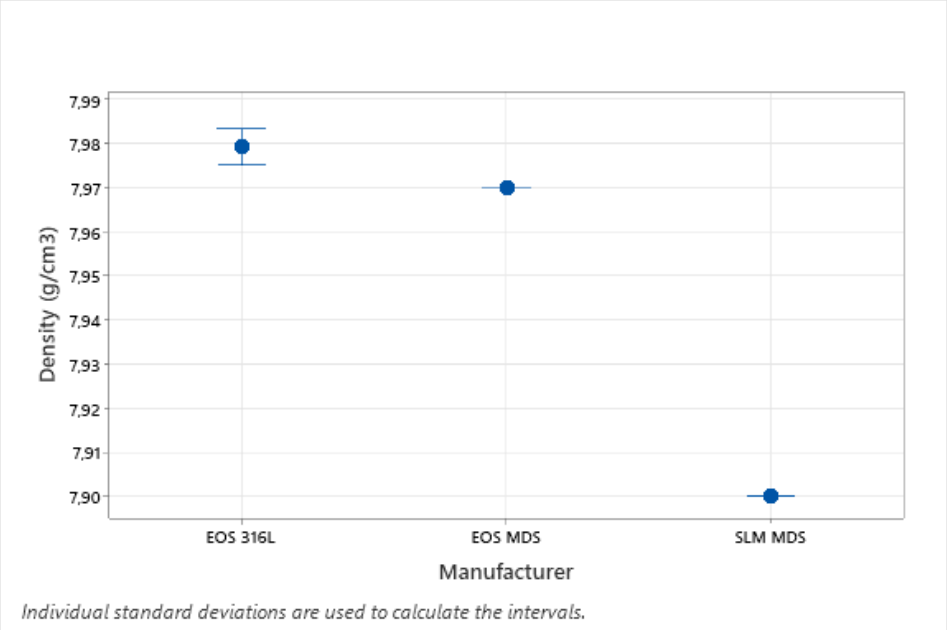

Figure 52. Density results of 316L samples compared to the MDS values

The density results of 316L can be seen in Figure 52. The results show that the density is comparable to the MDS value of EOS and higher than the density of 316L stated in the MDS of SLM. The density results reflect the results received from the porosity analysis, which show the minimal defect-% of the parts.

9 Conclusions

The basic principle of EOS M290 and the SLM 280HL are basically the same. However, they do have some differences between them that make a difference in the operating efficiency and comfort. The M290 is easier to work with than the 280HL in this configuration.

In regard to the first research question, how well can material feedstock be used in different systems, it can be said based on the results presented in this thesis, that material can be transferred to a third party system without major problems. As was seen in the results, some properties could be improved by further parameter optimisation, but in these cases, it is not required.

Considering the second research question: what changes in the infill parameters need to be done to get good results, the results showed that there is no real need to change the parameters as the results are such high quality on all three materials used in this thesis.

The third research question was: what it takes to create a new process for a system, it was found out that in this case the process creation was done using the Taguchi design with variable parameters. The process creation in this thesis was successful and no problems occurred as the parameters were discussed and designed with the help of experts from EOS.

Regarding the fourth and final research question: what are the key differences between systems and their operation, the main differences observed between the two systems are the differences in the powder handling. In these setups of the systems, the powder was inserted and taken out through the door of the process chamber in the M290, whereas on the 280HL, the powder was inserted through the roof of the system and taken out from the bottom.

In the case of the AlSi10Mg powder, it can be said that the experiments were a success, and the EOS powder can be used in the SLM280HL. Considering the results received from the experiments, EOS powder worked as good or even better in some cases than the SLM powder.

With MP1, the mechanical properties were good and thus the material can be used in the SLM machine. The surface roughness however could be improved by optimizing the surface parameters for MP1, as the received result on the roughness are not as good as they could be.

Using 316L in the 280HL was also made possible and successful with the experimented process parameters.

10 Further studies

Further studies could include the optimization of the heat treatment process for the EOS based AlSi10Mg manufactured in SLM machines. This could improve the properties of the finished components even more as the current heat treatment recipe is not optimized for the SLM parameters. The ageing time could be lowered from 6 hours to 4 hours as longer ageing times lower the elongation-%. (Pääkkönen, 2019)

The study could be continued by testing on a wider variety of materials to have the certainty that the materials can be used in multiple different systems. New systems should also be studied so that the materials could be used in as many systems as possible.

Some new studies with similar setup as in this thesis could also be conducted to get an even more conclusive answer on how well the materials work as well as testing more properties of the materials from the same setup. It is also suggested that the optimisation of certain parameters should be studies to achieve the optimal properties such as surface roughness.

References

Aboulkhair, N. T., Simonelli, M., Parry, L., Ashcroft, I., Tuck, C., & Hague, R. (2019). 3D printing of Aluminium alloys: Additive Manufacturing of Aluminium alloys using selective laser melting. *Progress in Materials Science*, *106*, 100578. https://doi.org/10.1016/j.pmatsci.2019.100578

Ahmed Obeidi, M., Uí Mhurchadha, S. M., Raghavendra, R., Conway, A., Souto, C., Tormey, D., Ahad, I. U., & Brabazon, D. (2021). Comparison of the porosity and mechanical performance of 316L stainless steel manufactured on different laser powder bed fusion metal additive manufacturing machines. *Journal of Materials Research and Technology*, *13*, 2361–2374. https://doi.org/10.1016/j.jmrt.2021.06.027

Altıparmak, S. C., Yardley, V. A., Shi, Z., & Lin, J. (2021). Challenges in additive manufacturing of high-strength aluminium alloys and current developments in hybrid additive manufacturing. *International Journal of Lightweight Materials and Manufacture*, *4*(2), 246–261. https://doi.org/10.1016/j.ijlmm.2020.12.004

ASTM International. (n.d.). *Standard for Additive Manufacturing – Finished Part Properties – Standard Specification for Cobalt-28 Chromium-6 Molybdenum via Powder Bed Fusion F3213-17*.

Bassoli, E., Defanti, S., Tognoli, E., Vincenzi, N., & Degli Esposti, L. (2021). Design for Additive Manufacturing and for Machining in the Automotive Field. *Applied Sciences*, *11*(16), 7559. https://doi.org/10.3390/app11167559

Boschetto, A., Bottini, L., & Pilone, D. (2021). Effect of laser remelting on surface roughness and microstructure of AlSi10Mg selective laser melting manufactured parts. *The International Journal of Advanced Manufacturing Technology*, *113*(9–10), 2739–2759. https://doi.org/10.1007/s00170-021-06775-3

Cao, L., Li, J., Hu, J., Liu, H., Wu, Y., & Zhou, Q. (2021). Optimization of surface roughness and dimensional accuracy in LPBF additive manufacturing. *Optics & Laser Technology*, *142*, 107246. https://doi.org/10.1016/j.optlastec.2021.107246

Choudhury, D., Ponneganti, S., Radhakrishnanand, P., Murty, U. S., & Banerjee, S. (2023). Selective laser sintering additive manufacturing of solid oral dosage form: Effect of laser power and hatch spacing on the physico-technical behaviour of sintered printlets. *Applied Materials Today*, *35*, 101943. https://doi.org/10.1016/j.apmt.2023.101943

Cortis, D., Pilone, D., Broggiato, G., Campana, F., Tatananni, D., & Orlandi, D. (2023, June 5). *Setting of L-PBF parameters for obtaining high density and mechanical performance of AISI 316L and 16MnCr5 alloys with fine laser spot size*.

D'Andrea, D. (2023). Additive Manufacturing of AISI 316L Stainless Steel: A Review. *Metals*, *13*(8), 1370. https://doi.org/10.3390/met13081370

Electro Optical Systems GmbH. (2024a). *EOS Aluminium AlSi10Mg Material Data Sheet*. https://www.eos.info/metal-solutions/metal-materials/aluminium

Electro Optical Systems GmbH. (2024b). *EOS Cobalt Chrome MP1 Material Data Sheet*. https://www.eos.info/metal-solutions/metal-materials/cobalt-chrome

Electro Optical Systems GmbH. (2024c). *EOS M290 brochure*. https://www.eos.info/metal-solutions/metal-printers/eos-m-290

Electro Optical Systems GmbH. (2024d). *EOS Stainless-Steel 316L Material Data Sheet*. https://www.eos.info/metal-solutions/metal-materials/stainless-steel

F42 Committee. (n.d.). *Standard for Additive Manufacturing Finished Part Properties Specification for AlSi10Mg with Powder Bed Fusion Laser Beam*. ASTM International. https://doi.org/10.1520/F3318

Ghio, E., & Cerri, E. (2022). Additive Manufacturing of AlSi10Mg and Ti6Al4V Lightweight Alloys via Laser Powder Bed Fusion: A Review of Heat Treatments Effects. *Materials*, *15*(6), 2047. https://doi.org/10.3390/ma15062047

Gor, M., Dobriyal, A., Wankhede, V., Sahlot, P., Grzelak, K., Kluczyński, J., & Łuszczek, J. (2022). Density Prediction in Powder Bed Fusion Additive Manufacturing: Machine Learning-Based Techniques. *Applied Sciences*, *12*(14), 7271. https://doi.org/10.3390/app12147271

Hegab, H., Khanna, N., Monib, N., & Salem, A. (2023). Design for sustainable additive manufacturing: A review. *Sustainable Materials and Technologies*, *35*, e00576. https://doi.org/10.1016/j.susmat.2023.e00576

Hitzler, L., Williams, P., Merkel, M., Hall, W., & Öchsner, A. (2017). Correlation between the Energy Input and the Microstructure of Additively Manufactured Cobalt-Chromium. *Defect and Diffusion Forum*, *379*, 157–165. https://doi.org/10.4028/www.scientific.net/DDF.379.157

Hong, J. H., & Yeoh, F. Y. (2020). Mechanical properties and corrosion resistance of cobalt-chrome alloy fabricated using additive manufacturing. *Materials Today: Proceedings*, *29*, 196–201. https://doi.org/10.1016/j.matpr.2020.05.543

Inovar Communications Ltd. (2023). *Metal AM Magazine Vol. 9 No. 4 Winter 2023*.

Karna, S. K. (n.d.). *An Overview on Taguchi Method*.

Kim, F. H., Moylan, S. P., Garboczi, E. J., & Slotwinski, J. A. (2017). Investigation of pore structure in cobalt chrome additively manufactured parts using X-ray computed tomography and three-dimensional image analysis. *Additive Manufacturing*, *17*, 23–38. https://doi.org/10.1016/j.addma.2017.06.011

Kleemeyer, S. D. (n.d.). *Determining the Influence of the Type of Shielding Gas during Additive Manufacturing of an Aluminum Alloy by Monitoring the Process Qualitatively and Analyz- ing Process Byproducts Quantitatively*.

Kotadia, H. R., Gibbons, G., Das, A., & Howes, P. D. (2021). A review of Laser Powder Bed Fusion Additive Manufacturing of aluminium alloys: Microstructure and properties. *Additive Manufacturing*, *46*, 102155. https://doi.org/10.1016/j.addma.2021.102155

Medrano, V. A., Arrieta, E., Merino, J., Ruvalcaba, B., Caballero, K., Ramirez, B., Diemann, J., Murr, L. E., Wicker, R. B., Godfrey, D., Benedict, M., & Medina, F. (2023). A comprehensive and comparative study of microstructure and mechanical properties for post-process heat treatment of AlSi7Mg alloy components fabricated in different laser powder bed fusion systems. *Journal of Materials Research and Technology*, *24*, 6820–6842. https://doi.org/10.1016/j.jmrt.2023.04.129

Michi, R. A., Plotkowski, A., Shyam, A., Dehoff, R. R., & Babu, S. S. (2022). Towards high-temperature applications of aluminium alloys enabled by additive manufacturing. *International Materials Reviews*, *67*(3), 298–345. https://doi.org/10.1080/09506608.2021.1951580

Mordas, G., Jasulaitienė, V., Steponavičiūtė, A., Gaspariūnas, M., Petkevič, R., Selskienė, A., Juškėnas, R., Paul, D. F., Mann, J. E., Remeikis, V., & Račiukaitis, G. (2020). Characterisation of CoCrMo powder for additive manufacturing. *The International Journal of Advanced Manufacturing Technology*, *111*(11–12), 3083–3093. https://doi.org/10.1007/s00170-020-06236-3

Moshiri, M., Candeo, S., Carmignato, S., Mohanty, S., & Tosello, G. (2019). Benchmarking of Laser Powder Bed Fusion Machines. *Journal of Manufacturing and Materials Processing*, *3*(4), 85. https://doi.org/10.3390/jmmp3040085

Muñoz, V. (2017). *Analysis of the optimal parameters for 3D printing aluminum parts with a SLM 280 machine*.

Pääkkönen, I. (2019). *Optimization of heat treatment of additively manufactured aluminum silicon alloys*.

Peng, T., Kellens, K., Tang, R., Chen, C., & Chen, G. (2018). Sustainability of additive manufacturing: An overview on its energy demand and environmental impact. *Additive Manufacturing*, *21*, 694–704. https://doi.org/10.1016/j.addma.2018.04.022

Reijonen, J., Revuelta, A., Riipinen, T., Ruusuvuori, K., & Puukko, P. (2020). On the effect of shielding gas flow on porosity and melt pool geometry in laser powder bed fusion additive manufacturing. *Additive Manufacturing*, *32*, 101030. https://doi.org/10.1016/j.addma.2019.101030

Revilla, R. I., Van Calster, M., Raes, M., Arroud, G., Andreatta, F., Pyl, L., Guillaume, P., & De Graeve, I. (2020). Microstructure and corrosion behavior of 316L stainless steel prepared using different additive manufacturing methods: A comparative study bringing insights into the impact of microstructure on their passivity. *Corrosion Science*, *176*, 108914. https://doi.org/10.1016/j.corsci.2020.108914

Rosenthal, I., Shneck, R., & Stern, A. (2018). Heat treatment effect on the mechanical properties and fracture mechanism in AlSi10Mg fabricated by additive manufacturing selective laser melting process. *Materials Science and Engineering: A*, *729*, 310–322. https://doi.org/10.1016/j.msea.2018.05.074

SLM Solutions. (2024). *SLM 280HL brochure*. https://nikon-slm-solutions.com/slm-systems/

Sola, A., & Nouri, A. (2019). Microstructural porosity in additive manufacturing: The formation and detection of pores in metal parts fabricated by powder bed fusion. *Journal of Advanced Manufacturing and Processing*, *1*(3), e10021. https://doi.org/10.1002/amp2.10021

Tolvanen, E. (2024). *Effect of laser beam angle of incidence on surface roughness and porosity of IN718 parts manufactured via laser powder bed fusion*.

Uriati, F., & Nicoletto, G. (2022). A comparison of Inconel 718 obtained with three L-PBF production systems in terms of process parameters, as-built surface quality, and fatigue performance. *International Journal of Fatigue*, *162*, 107004. https://doi.org/10.1016/j.ijfatigue.2022.107004

Vafadar, A., Guzzomi, F., Rassau, A., & Hayward, K. (2021). Advances in Metal Additive Manufacturing: A Review of Common Processes, Industrial Applications, and Current Challenges. *Applied Sciences*, *11*(3), 1213. https://doi.org/10.3390/app11031213

Vastola, G., Pei, Q. X., & Zhang, Y.-W. (2018). Predictive model for porosity in powder-bed fusion additive manufacturing at high beam energy regime. *Additive Manufacturing*, *22*, 817–822. https://doi.org/10.1016/j.addma.2018.05.042

Volpato, G. M., Tetzlaff, U., & Fredel, M. C. (2022). A comprehensive literature review on laser powder bed fusion of Inconel superalloys. *Additive Manufacturing*, *55*, 102871. https://doi.org/10.1016/j.addma.2022.102871

Whip, B., Sheridan, L., & Gockel, J. (2019). The effect of primary processing parameters on surface roughness in laser powder bed additive manufacturing. *The International Journal of Advanced Manufacturing Technology*, *103*(9–12), 4411–4422. https://doi.org/10.1007/s00170-019-03716-z

Wu, A. S., Brown, D. W., Kumar, M., Gallegos, G. F., & King, W. E. (2014). An Experimental Investigation into Additive Manufacturing-Induced Residual Stresses in 316L Stainless Steel. *Metallurgical and Materials Transactions A*, *45*(13), 6260–6270. https://doi.org/10.1007/s11661-014-2549-x

Yang, D., Huang, Y., Fan, J., Jin, M., Peng, Y., & Wang, K. (2021). Effect of N2 content in shielding gas on formation quality and microstructure of high nitrogen austenitic

stainless steel fabricated by wire and arc additive manufacturing. *Journal of Manufacturing Processes*, *61*, 261–269. https://doi.org/10.1016/j.jmapro.2020.11.020

Yonehara, M., Ikeshoji, T.-T., Nagahama, T., Mizoguchi, T., Tano, M., Yoshimi, T., & Kyogoku, H. (2020). Parameter optimization of the high-power laser powder bed fusion process for H13 tool steel. *The International Journal of Advanced Manufacturing Technology*, *110*(1–2), 427–437. https://doi.org/10.1007/s00170-020-05879-6

Zhang, Z., Wang, S., Liu, H., Wang, L., & Xiao, X. (2023). Effects of Hatch Distance on the Microstructure and Mechanical Anisotropy of 316 L Stainless Steel Fabricated by Laser Powder Bed Fusion. *Journal of Materials Engineering and Performance*, *32*(10), 4757–4767. https://doi.org/10.1007/s11665-022-07416-w

Appendices

Furnace: UUN8
Program name: 010 530C Solution annealing
Start Date/Time: 18.6.2024 11.06.59
File name: UUN8_2024-6-18_11-06-59.archive

Diagram:

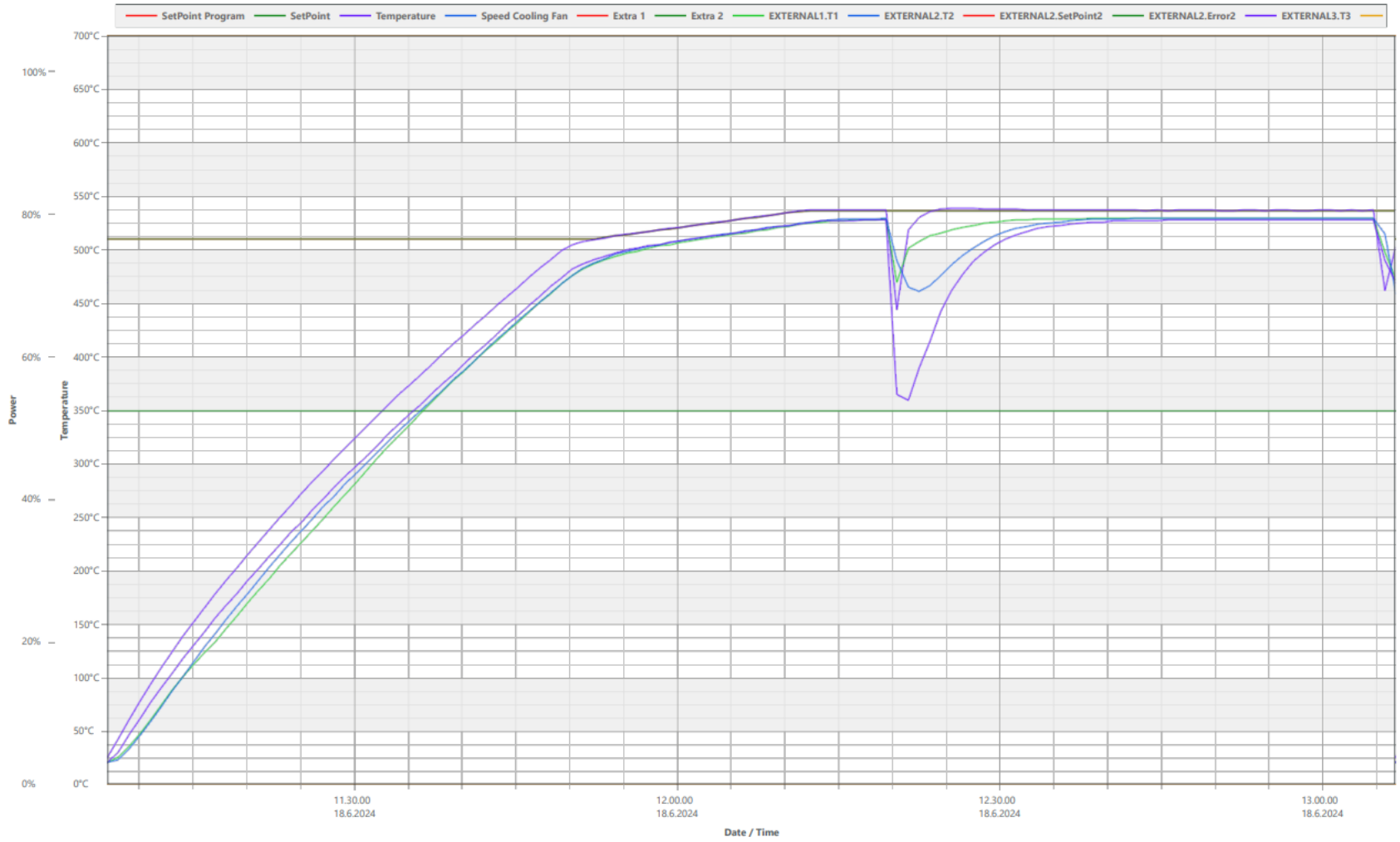

Furnace: UUN8
Program name: 012 AlSi10Mg, T6 Aging
Start Date/Time: 19.6.2024 6.30.19
File name: UUN8_2024-6-19_06-30-19.archive

Diagram: